REVMAT 2 (2026) 100252

Contents lists available at ScienceDirect

Review of Materials Research

journal homepage: www.sciencedirect.com/journal/review-of-materials-research

Concise Review

Thermal transport at reduced dimensions: From fundamentals to functional materials

Wenyang Ding, Bingyang Cao *

Key Laboratory for Thermal Science and Power Engineering of Ministry of Education, Department of Engineering Mechanics, Tsinghua University, Beijing, 100084, China

ARTICLE INFO

Keywords:
Nanoscale thermal transport
2D materials
vdW heterostructures
Materials informatics

ABSTRACT

As device dimensions shrink and power densities increase in post-Moore electronics, thermal transport has become a critical challenge for next-generation technologies. At reduced dimensions, classical Fourier heat conduction becomes inadequate due to phonon confinement, interface scattering, and quantum effects. This review summarizes recent advances in phonon-mediated thermal transport in low-dimensional materials, particularly two-dimensional (2D) materials and van der Waals (vdW) heterostructures. Fundamental mechanisms, including phonon scattering, dimensional confinement, and interfacial thermal resistance, are discussed together with representative 2D systems such as graphene, hexagonal boron nitride, transition metal dichalcogenides, and black phosphorus. Particular attention is devoted to interfacial thermal transport and twist-angle-dependent phonon engineering in vdW heterostructures, which enable effective control of thermal transport through tunable interlayer coupling. Emerging phenomena, including phonon hydrodynamics and asymmetric thermal transport, are also highlighted. In addition, the growing role of materials informatics and machine learning in designing thermal functional materials is discussed. By connecting fundamental phonon physics with data-driven materials engineering, this review provides perspectives for thermal management, thermoelectric energy conversion, and next-generation energy-efficient technologies.

1. Introduction

In the post-Moore era, as device dimensions shrink and power densities surge, localized hotspots and inefficient heat dissipation severely threaten the performance and reliability of electronic components. Thermal management has become a critical bottleneck across a broad spectrum of advanced technologies, from next-generation microelectronics to aerospace and energy systems [1–4]. At the micro- and nanoscales, however, classical Fourier-based descriptions of heat conduction break down [5]. Heat carriers such as phonons undergo boundary scattering, size confinement, and quantum effects, giving rise to transport behaviors that deviate strongly from bulk predictions.

Low-dimensional materials, such as, graphene, hexagonal boron nitride (*h*-BN), transition metal dichalcogenides (TMDs), and black phosphorus (BP), provide an unprecedented opportunity to explore and harness non-classical phenomena, offering promising routes for addressing diverse application needs. Moreover, a particularly exciting attention originates from the rise of two-dimensional (2D) van der Waals (vdW) heterostructures, in which atomically thin layers are vertically stacked without the constraint of lattice matching. These systems combine diverse electronic, optical, and thermal characteristics, while their weak interlayer interactions allow unprecedented control over interfacial phonon coupling. Recent studies demonstrated that vdW heterostructures can be engineered through stacking sequence [1,6], twist angle [7–10], and strain [11] to achieve tailored thermal conductivity ranging from ultralow values desirable for thermoelectrics to high interfacial thermal conductance essential for heat dissipation [4]. For example, in graphene/WS_2 heterostructures, understanding the role of critical incident angles and phonon tunneling in suppressing cross-plane heat transport enabled the optimization of stacking sequences, leading to the discovery of structures with ultralow thermal conductivity [12]. This example highlights how fundamental insights into phonon transport can guide rational material design and ultimately enable targeted thermal functionalities. Such capability establishes vdW heterostructures as a promising class of thermal functional materials.

The rapid development of advanced characterization and computational techniques have substantially advanced our capability to probe and predict heat conduction properties across multi scales, such as 3ω-

* Corresponding author
E-mail address: caoby@mail.tsinghua.edu.cn (B. Cao).

https://doi.org/10.1016/j.revmat.2026.100252
Received 20 May 2026; Received in revised form 9 July 2026; Accepted 3 August 2026
Available online 4 August 2026

method [13], time-domain thermoreflectance (TDTR) [14], suspended micro-bridge [15], optothermal Raman techniques [16] and machine learning algorithm [17] enable direct visualization of heat dissipation at nanometer resolution, while molecular dynamics (MD) simulations employing empirical force fields [18] and machine-learning potential [19–21], first-principles methods [22], and atomistic Green's function (AGF) methods [23] have provided fundamental phonon transport governed by the wave-particle duality of phonons. Together, these advances provide an integrated framework for understanding and manipulating thermal transport at reduced dimensions. Complementing these physics-based approaches, materials informatics (MI) are emerging as powerful tools to accelerate the discovery and optimization of 2D materials and vdW heterostructures, with machine learning (ML) playing a central role. By mining large datasets and building predictive models, ML provides a complementary route to unravel structure-property relationships and guide the design of materials with targeted thermal performance.

In this review, we provide a comprehensive overview of thermal transport at reduced dimensions, with a particular emphasis on 2D materials and vdW heterostructures. We summarize the fundamental mechanisms, highlight advances, and discuss emerging data-driven strategies for tailoring heat flow at the atomic scale. By linking fundamental insights with application-driven needs in microelectronics, aerospace, power electronics, and thermoelectrics, this review aims to illuminate both the challenges and opportunities of nanoscale thermal science in shaping the technologies of the future.

2. Fundamentals and recent advances

2.1. Heat transport in bulk scale

Heat conduction refers to the transfer of thermal energy within a material driven by temperature gradients, arising from the random motion of heat carriers such as molecules, electrons, or phonons. In this process, the material serves as the medium through which energy is transported from regions of high temperature to low temperature. The macroscopic description of heat conduction is commonly based on Fourier's law [24–26].

$$q = -\kappa \nabla T \tag{1}$$

where κ denotes the thermal conductivity and has units of [W/m-K]. Units of q is [Wm^{-2}]. ∇ is the gradient operator that works as

$$\nabla T = \frac{\partial T}{\partial x}\hat{x} + \frac{\partial T}{\partial y}\hat{y} + \frac{\partial T}{\partial z}\hat{z} \tag{2}$$

where $\hat{x}$, $\hat{y}$ and $\hat{z}$ are the unit vectors along coordinate directions. The thermal conductivity of a material fundamentally determines its capacity for heat transport, with larger values indicating superior heat conduction capabilities.

Fig. 1 illustrates the wide-ranging thermal conductivity of materials at room temperature [25]. In a vacuum, insulators can display remarkably ultralow thermal conductivity, reaching around $\sim 10^{-3}$ W/m-K. Gases also generally exhibit significantly lower thermal conductivity. Thermal conductivities of woods and polymers usually are around 0.1 W/m-K, about ten times smaller than water and glass [24–26]. Thermal conductivities of semiconductors (such as silicon) are 156 W/m-K [27]. Remarkably, carbon allotropes, especially diamond, stand out for their exceptional thermal conductivities, surpassing those of highly conductive metals like copper. Notably, recently developed materials like cubic boron arsenide crystals demonstrate thermal conductivity of about 1000 W/m-K, rivaling those of diamond [28–31].

Thermal transport mainly relies on the movement and collisions of heat carriers within a system. The heat carriers and the mechanism of heat conduction for these materials are quite different. In gases as shown in Fig. 2 (a), gas molecules near the hot wall frequently collide with the

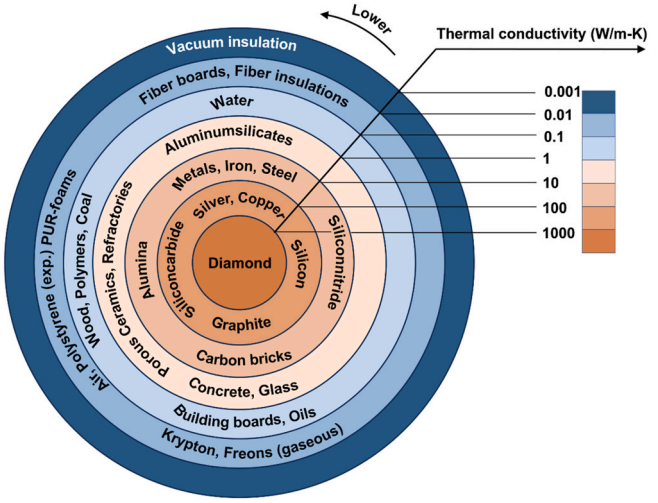

Fig. 1. Thermal conductivity for different materials at room temperature.

solid atoms, which lead to the increase of their kinetic energy or random velocity. These molecules, engaged in random motion, have the potential to move towards the lower temperature end. Throughout this process, they collide with molecules possessing lower random velocities (and thus cooler temperatures), transferring excess energy to those molecules. This cascading process continues for all adjacent molecules until it reaches those in the vicinity of the cold wall. These molecules, with higher kinetic energy than the atoms in the solid wall, transmit their excess energy to the wall through collisions. The cumulative effect is a pure energy flow from the hot wall to the cold wall, driven by the temperature disparity between the two walls. We need to note that the pure energy flow is a result of the random motion of molecules, and they don't need really transition from the hot side to the cold side [32,33].

The formation of a metal involves atoms bonding together, releasing some electrons from the outer orbits of the nuclei. These liberated electrons, unbound by interatomic forces, can traverse distances significantly greater than interatomic spacings until they encounter scattering events with atoms, other electrons, or impurities. Conceptually, these free electrons can be envisioned as constituting a gas as shown in Fig. 2 (b). Free electrons in metals exhibit significantly high velocity. Consequently, heat transport in metals is primarily dominated by electrons [34,35].

Within dielectric solid materials and lightly/moderately doped semiconductors, heat propagation occurs through the vibrational motion of atoms. These atoms are interconnected in the dielectric material through interatomic force interactions. Fig. 2 (c) is a schematic representation of the interatomic potential energy, denoted as ϕ, plotted against the interatomic distance, x, between two atoms. The force interaction between these atoms is derived from the gradient of the interatomic potential.

$$F = \frac{-d\phi}{dx} \tag{3}$$

when two atoms are far away from each other, the electrons of one atom would attract the nucleus of the other atom, which leads to an attractive force. As the atoms draw closer, the interaction force transitions to a repulsive state because the electron orbits or nuclei of different atoms begin to overlap. The equilibrium positions of the atoms are determined by the lowest potential. Each solid's atom vibrates around its respective equilibrium position, with its motion influenced by neighboring atoms through interatomic potential. A simplified representation of interatomic interaction in crystals involves a mass-spring system, depicted in Fig. 2 (d). In this system, the vibration of a single atom can induce vibrations throughout the entire system by generating lattice waves.

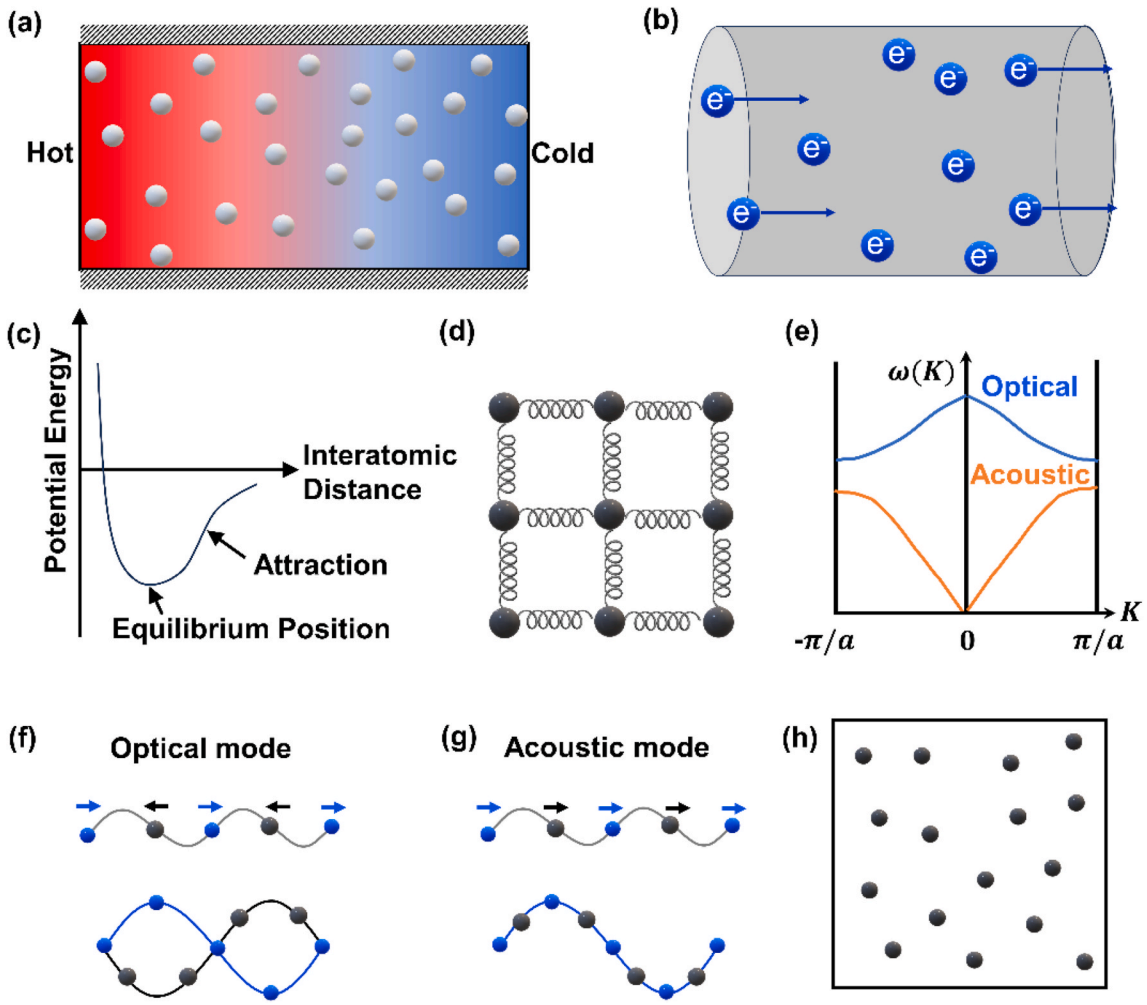

Fig. 2. The mechanism of heat conduction for different phases of materials. (a) Heat carriers and conduction mechanism in gases, (b) Free electrons conceptualized as forming an electron gas, (c) Schematic of the interatomic potential in dielectric solids, (d) Simplified representation of interatomic interaction in crystals using a mass-spring system, (e) These modes are defined by wavevectors K and frequencies ω within the Brillouin zone, defined by $\pm\pi/a$, (f) Optical phonons modes, describing vibrations in which neighboring atoms moving in alternating directions, (g) Acoustic phonons modes, describing vibrations that move nearly synchronously due to their low frequency, (h) Illustration of phonon particles.

Quantum mechanics dictates that the energy of each lattice wave must be discrete, a multiple of $h\nu$ (except for a small modification known as zero-point energy). In this context, ν means lattice wave's frequency while h represents Planck constant (6.6×10^{-34} J · s). This minimum energy, $h\nu$, of a quantized lattice wave is termed a phonon. A phonon state, more commonly referred to as a phonon mode, is a vibrational wave within a crystalline solid of a specific wavevector and frequency. This can be represented conveniently in the dispersion relation, which relates phonon mode energy to wavevector, as shown in Fig. 2 (e), for a diatomic chain.

The occupation of phonon is determined by the Bose-Einstein distribution reproduced in equation (4),

$$\langle n_{K,p}\rangle = \frac{1}{\exp\left(\frac{\hbar\omega_{K,p}}{k_B T}\right) - 1} \tag{4}$$

Here, $\langle n_{K,p}\rangle$ represents the number of phonons that occupy a state of wavevector K and polarization p. ω-Phonon state energy, $\hbar$-reduced Planck constant, k_B-Boltzmann constant, and T-absolute temperature.

The heat capacity at constant volume is defined as

$$C_V \equiv \left(\frac{\partial U}{\partial T}\right)_V \tag{5}$$

where U is the system internal energy and T is the absolute temperature. The contribution of phonons to heat capacity (sometimes referred to as lattice heat capacity) is quantified based on the lattice energy:

$$U_{lat} = \sum_K \sum_p \langle n_{K,p}\rangle \hbar\omega_{K,p} \tag{6}$$

The summation over wavevectors may be replaced so that the expression is written in terms of the change in the quantity of modes per change in energy level, otherwise known as the density of states $D_p(\omega)$.

$$U_{lat} = \sum_p \int d\omega D_p(\omega) \frac{\hbar\omega}{\exp\left(\frac{\hbar\omega_{K,p}}{k_B T}\right) - 1} \tag{7}$$

If the substitution of $x = \frac{\hbar\omega}{k_B T}$ is made, Equation (4) can be used to determine the lattice heat capacity:

$$C_{V,lat} = k_B \sum_p \int d\omega D_p(\omega) \frac{x^2 \exp(x)}{[\exp(x) - 1]^2} \tag{8}$$

The Debye model for the density of states relates the dispersion relation to the wavevector linearly via the speed of sound, which is constant across all polarizations, such that $\omega = \nu K$. Therefore, the density of states is

$$D(\omega) = \frac{dN}{d\omega} = \frac{VK^2}{2\pi^2}\frac{dK}{d\omega} = \frac{V\omega^2}{2\pi^2 v^3} \tag{9}$$

where N represents the number of modes having a wavevector equal to or less than K and V represents the volume of the model system. If the phonon velocity is independent of polarization, then the summation in equation (8) can be replaced by a factor of 3. Once this is done, the expression becomes

$$C_{V,lat} = 9Nk_B\left(\frac{T}{\theta}\right)^3 \int_0^{\frac{\theta}{T}} dx \frac{x^4 e^x}{(e^x-1)^2} \tag{10}$$

where θ represents the Debye temperature, or the temperature at which the highest frequency acoustic phonon mode become occupied:

$$\theta = \frac{\hbar v}{k_B}\left(\frac{6\pi^2 N}{V}\right)^{\frac{1}{3}} \tag{11}$$

The Debye temperature of a material is a key characteristic that generally represents the upper limit for phonon excitation. At temperatures around or below this scale, high-frequency optical modes, as illustrated in Fig. 2 (f), may remain weakly excited. Compared with acoustic modes (Fig. 2 (g)), these optical modes typically contribute less to heat capacity and thermal conductivity, and therefore play a secondary role in heat transport. Accordingly, the Debye temperature provides a useful metric for describing heat storage and transport behavior in non-metallic materials.

2.2. Nanoscale heat transport

In contemporary devices, including computer chips, characteristic sizes have been scaled down to the micrometer and nanometer regimes. The conventional continuum models fail to capture the complexities of heat transport and storage phenomena at this scale [5]. However, nanoscale thermal control constitutes a fundamental aspect of the design for emerging devices in fields such as electronics, electro-optics, thermoelectric, and photovoltaics. Therefore, researchers delve into analyses and experiments grounded in nanoscale perspectives, which not only enhance our comprehension of thermal transport in modern technologies but also find applicability in challenging scenarios, such as extreme temperatures and intricate structures, where traditional approaches encounter difficulties.

The impact of nanoscale heat transfer research resonates across various engineering, materials science, and chemistry domains. A notable breakthrough occurred when researchers managed to suspend a single-walled carbon nanotube between two metal contacts, yielding an exceptional thermal conductivity of 3500 W/m-K [36]. This achievement was previously hindered by constraints in carbon nanotube synthesis and nanofabrication techniques available at the time. The researchers attributed the observed trend to a synergistic interplay of Umklapp scattering and three phonon scattering processes [37]. Adopting a comparable methodology, a different research team gauged the thermal conductivity of single-layer graphene, revealing an impressive value of 5300 W/m-K [38]. In contrast, innovative non-contact laser techniques have facilitated the identification of materials with exceptionally low thermal conductivity. Utilizing TDTR, a study delved into the thermal conductivity of WSe_2, unveiling an extraordinarily low figure of 0.05 W/m-K [39]. Employing analogous techniques, other research teams have assessed the thermal conductivity of the fullerene derivative PCBM, pinpointing a value below 0.06 W/m-K due to scattering mechanisms within the amorphous regime [40–42]. While experimental measurements provide quantitative values of thermal conductivity, interpreting these results requires an understanding of lattice vibrations, or phonons, and their scattering mechanisms.

Thermal conductivity due to phonons (otherwise sometimes called lattice thermal conductivity) is related to their velocity and scattering rate. As we introduced before, the energy of these harmonic vibrations is quantized. Each quantum of this quantized energy is referred to as a harmonic vibrational energy quantum, commonly known as a phonon. However, when the magnitude of atomic oscillations around their equilibrium points grows larger, the harmonic approximation (second-order approximation) becomes invalid. In such cases, we need to consider higher-order interaction terms, which include phonon-phonon interactions. The simplest interaction model in this scenario is the three-phonon process. In this model, the first phonon and the second phonon collide to produce the third phonon while maintaining the conservation of energy and momentum throughout the process:

$$\hbar\omega_1 + \hbar\omega_2 = \hbar\omega_3 \tag{12}$$

$$\hbar\vec{q}_1 + \hbar\vec{q}_2 = \hbar\vec{q}_3 + \hbar\vec{G} \tag{13}$$

where G is the reciprocal lattice vector. Physically, this type of collision means that the influence of one lattice wave on the crystal lattice affects another lattice wave, thereby generating a third lattice wave. If two phonons collide and their combined wavevector remains within the first Brillouin Zone, the reciprocal lattice vector is zero. This process is called normal scattering, which does not generate thermal resistance [43]. If the combined third wavevector created by the collision of the two phonons escapes from the first Brillouin Zone, the reciprocal lattice vector is non-zero. This process is called Umklapp process. In this case, the resulting phonon experiences a significant change in its direction compared to the original two phonons, leading to large-angle scattering and thus generating thermal resistance. This Umklapp process is a key mechanism for generating heat flow, as the total wavevector of all phonons is no longer zero.

However, thermal transport is often not solely limited by phonon-phonon scattering. Instead, phonons can be scattered by defects [44,45], interfaces [46,47], impurities [20,48], and boundaries. Additionally, phonons may be scattered by other heat carriers such as electrons and holes [49]. The overall scatter effects from different sources are described by Matthiessen's rule:

$$\frac{1}{\tau} = \frac{1}{\tau_{\text{Umklapp}}} + \frac{1}{\tau_{\text{impurities,defects}}} + \frac{1}{\tau_{\text{boundary}}} + \frac{1}{\tau_{\text{phonon-electron}}} \tag{14}$$

where τ is phonon relaxation time. The boundary scattering behavior of phonons is influenced by relationship between characteristic length scales of phonons and system size.

Heat conduction is the diffusive nature of thermal energy transport due to the random motion and consequent collision of heat carriers (which are primarily phonons in semiconductors). Therefore, gases' kinetic theory can be used to develop an expression for thermal conductivity:

$$k = \frac{1}{3}C_V\bar{v}\bar{\Lambda} \tag{15}$$

where $\bar{v}$ is the average phonon velocity and $\bar{\Lambda}$ is the average mean free path of all active phonons. Equation (13) can be substituted into the Fourier law (equation (1)) to create an equation that describes conductive heat flux in terms of a phonons gas [35].

$$q = -\frac{1}{3}C_V v\Lambda\nabla T \tag{16}$$

Equation (14) presumes isotropic thermal transport in each direction, which is the basis of understanding heat transfer in the complex material systems.

Recent years have witnessed remarkable progress in phonon transport studies in low-dimensional materials, extending beyond the conventional diffusive transport framework. Besides ballistic and hydrodynamic transport [50], emerging transport phenomena such as

superdiffusive heat conduction [51] and second sound [52] have attracted considerable attention. Recent theoretical and atomistic studies have demonstrated that phonon confinement and enhanced momentum-conserving normal scattering can induce collective phonon dynamics [53,54], providing new insights into the microscopic origin of non-Fourier heat conduction. Meanwhile, significant advances have also been made in the active manipulation of phonon transport through artificially engineered phononic structures. Phononic metamaterials, including metagratings and superlattice architectures [55], have been shown to enable asymmetric phonon transmission and directional heat transport, opening new opportunities for realizing phononic devices with tailored thermal functionalities. These recent developments not only deepen the fundamental understanding of collective phonon transport in low-dimensional materials but also provide promising strategies for phonon engineering and nanoscale thermal management.

2.2.1. Interfacial thermal transport

It is indicated that the microscopic structure presented at solid contacts are crucial factors limiting thermal transport across these contacts [56]. Thermal resistance at the contact layer has become a technical bottleneck for many modern high-tech applications, such as the integration and performance of large-scale integrated chips. Enhancing thermal transport across these contact layers can directly improve device performance. Due to the complexity and uncertainty of contact interfacial thermal resistance, the study of thermal transport characteristics at solid-solid contact interfaces has emerged as a challenging problem in the science of thermal transport.

When two solid materials come into contact, the interfacial heat transfer is influenced by multiple factors. Recent studies on nano-carbon assemblies and thermal interface materials have highlighted that interfacial thermal transport can be effectively regulated through interface engineering, underscoring the critical role of contact structure in determining thermal resistance [57,58]. Interfacial geometry plays a key role, including surface roughness [59], vacancy defects [60], lattice orientation [61], nano-inclusions [62], and interfacial adhesion or bonding [63]; Material properties also affect heat transfer, encompassing the thermal characteristics of the contacting materials as well as any interstitial media [64,65]; In addition, the interface contact status, such as the presence of relative sliding, can also modify thermal transport. Beyond these factors, load conditions (such as contact pressure and the history of loading), and temperature conditions (such as the average temperature of the contact surfaces, heat flux density and direction, and the history of temperature changes) also play significant roles.

Many of these factors are nonlinear, which creates coupling interactions that further complicate the issue. Specifically, if there are multiple interfaces in structure, the problem will become more complex. For example, in superlattices, multiple interfaces lead to constructive and destructive phonon interference as well as resonance effects. In nanostructures, there are a high density of interfaces, which could reflect phonons instead of letting them transmitted, leading to thermal resistance.

Therefore, understanding interfacial heat transfer has always been challenging. The initial theoretical understanding of interfacial heat transfer began with the Acoustic Mismatch Model (AMM) as shown in Fig. 3 (a) and the Diffuse Mismatch Model (DMM) as shown in Fig. 3 (b). The AMM assumes that phonons propagate as sound waves at the interface between two materials. The model assumes that phonons are reflected or refracted in the form of elastic waves and that the interface is perfect, without any defects or roughness. AMM is based on several key assumptions: the interface is smooth and defect-free, meaning there are no irregularities or roughness; Phonons are transmitted as elastic waves, following the laws of elastic mechanics; Energy and momentum are conserved, meaning that energy and momentum are conserved at the interface during phonon propagation; and There is angular dependence, meaning the reflection and refraction of phonons depend on the angle of incidence. AMM is mainly applicable to phonon transport at low temperatures and low frequencies, where the phonon wavelength is long and the geometric features of the interface have minimal impact on heat transfer. The DMM assumes that phonon transport at the interface is random, and phonon scattering at the interface is diffuse. This means that phonon reflection and transmission at the interface are no longer elastic and deterministic but follow statistical probabilities. The assumptions of this model include: The interface is rough and has defects, meaning the interface is no longer perfect and there is surface roughness and structural mismatch; Phonon scattering is random, meaning phonon behavior at the interface is random and follows a statistical distribution; energy is conserved, but momentum conservation is not required, meaning that the phonon momentum at the interface may change direction. DMM is more applicable to high-temperature conditions or high-frequency phonon transport, as in these conditions, the phonon wavelength is shorter and the microstructure of the interface significantly affects the phonon propagation path. These two models provide a theoretical foundation for studying and understanding heat transfer at the interfaces of different materials, although their applicability conditions differ.

The DMM and AMM are based on the phonon gas model, which assumes a perfectly periodic lattice. However, real interfaces often have significant structural disorder, conflicting with this assumption of perfect periodicity. As a result, these models cannot account for the structural details at the interface and instead calculate phonon transmission

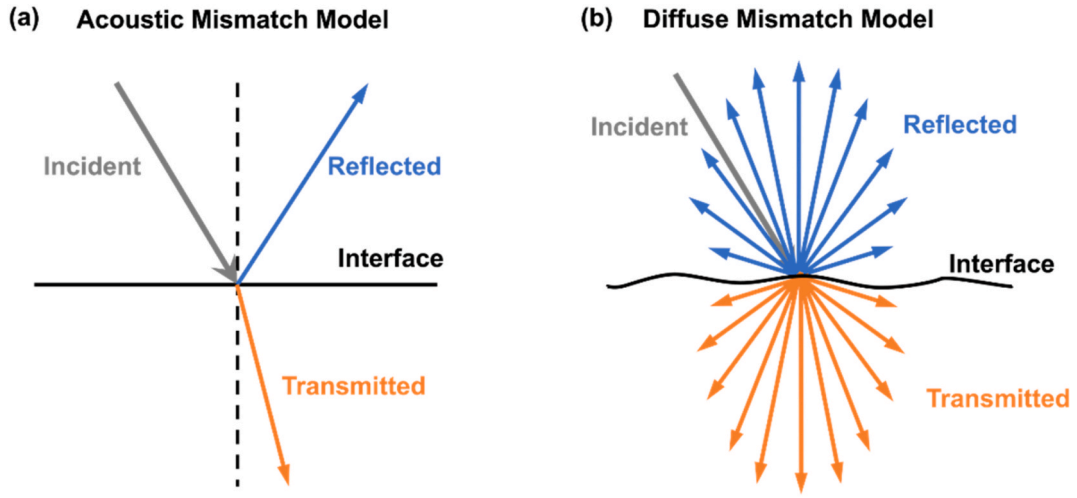

Fig. 3. Schematics of (a) AMM and (b) DMM.

based solely on the phonon properties of the two materials forming the interface. The later-developed AGF method can consider the details of the interface but struggles to account for the effects of inelastic processes on interfacial thermal conduction and involves extensive computational demands. With the application of MD in interfacial heat transfer calculations, the contribution of inelastic processes to interfacial thermal conductivity can be assessed. Richer vibrational modes, known as interfacial phonon states, are predicted at the interface. These states are entirely different from the bulk phonon properties of the materials forming the interface and have significant direct and indirect contributions to interfacial heat transfer. Recent progress has been made in the theoretical prediction and experimental verification of interfacial phonon states. However, MD calculations are based on classical mechanics and cannot account for quantum effects, which can significantly impact predictions of interfacial thermal conductivity at low temperatures.

Although substantial progress has been achieved in understanding interfacial thermal transport, no existing theoretical framework can fully describe heat transfer across realistic interfaces. The classical AMM and DMM provide intuitive physical pictures for idealized coherent and incoherent phonon transmission, respectively, but neglect the structural complexity of practical interfaces. The AGF method extends the description by explicitly incorporating atomic-scale interfacial structures and coherent phonon transport, yet its applicability is largely restricted to harmonic systems and becomes computationally demanding for realistic materials. Molecular dynamics simulations overcome this limitation by naturally capturing anharmonicity and inelastic phonon scattering, enabling direct investigations of interfacial phonon states and their contributions to thermal transport. Nevertheless, the classical nature of MD limits its predictive capability at low temperatures where quantum statistics become important.

These complementary approaches highlight that interfacial thermal transport cannot be fully understood within a single theoretical framework. Future developments are expected to integrate first-principles calculations, atomistic simulations, and data-driven approaches to bridge multiple length and time scales. In particular, machine-learning interatomic potentials [66] and AI-assisted multiscale modeling are emerging as promising tools to simultaneously achieve high accuracy and computational efficiency for predicting thermal transport across structurally complex interfaces. Such advances will not only deepen the fundamental understanding of interface-dominated heat conduction but also provide practical guidance for designing next-generation thermal interface materials and heterogeneous electronic devices.

2.2.2. *Thermal properties of 2D materials*

2.2.2.1. Thermal conductivity of 2D materials. In 2004 [67], graphene captured widespread attention due to its unique 2D planar structure and large specific surface area, which endowed it with exceptional properties [68–70]. These properties enabled breakthroughs in several fields and triggered intensive research into 2D materials. Subsequently, a variety of other 2D materials have been extensively explored, including *h*-BN, SnSe, BP, MoS_2, and Bi_2Te_3 as shown in Fig. 4. Starting from graphene, 2D materials have evolved into a diverse family encompassing conductors, semiconductors, superconductors, and insulators. Initially studied for their transport properties, 2D materials have permeated many fields, such as optoelectronic and spintronic devices, and have expanded into new areas such as photocatalysts, electrocatalysts, lithium-ion batteries, solar cells, and supercapacitors. They hold promise for widespread application in next-generation information transmission devices and energy storage technologies. To date, various techniques have been developed to produce atomically thin 2D materials, including mechanical exfoliation [67,76,77], liquid-phase exfoliation [78,79] and chemical vapor deposition [80–82]. The advancement of synthesizing 2D materials with high-quality and the development of thermal transport measurement techniques for low-dimensional materials offer a solid foundation to investigate thermal properties of 2D materials. Hence, thermal transport in 2D materials, including few-layer graphene [38,83–86], *h*-BN [87,88], MoS_2 [89,90], BP [91,92], and Bi_2Te_3 [93], has been extensively studied in recent years.

Graphene is a representative of 2D nanomaterial. A suspended

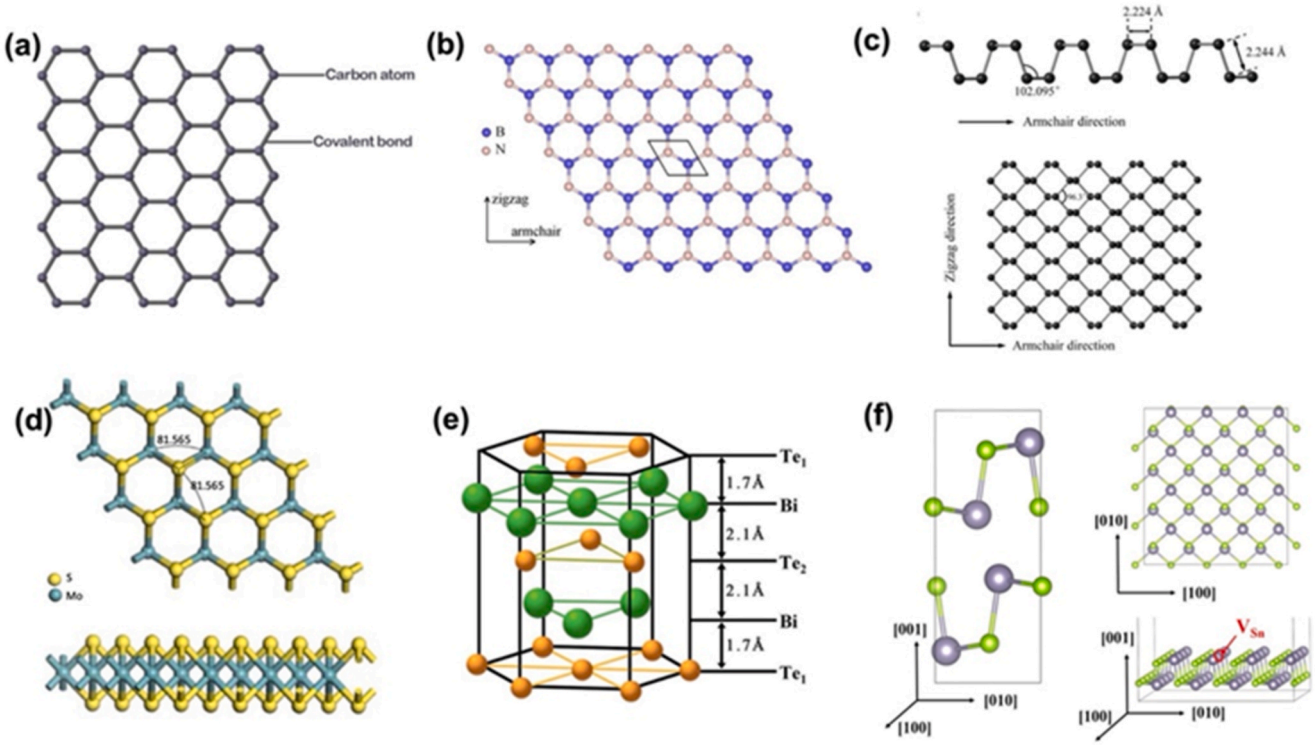

Fig. 4. Schematic of 2D materials: (a) graphene, (b) *h*-BN [71], (c) BP [72], (d) MoS_2 [73], (e) Bi_2Te_3 [74], (f) SnSe [75].

single-layer graphene's thermal conductivity has been reported as 5300 W/m-K [38]. This value is much higher than that in highly oriented bulk pyrolytic graphite and diamond. However, this value is obtained without considering the effect of substrate and contact resistance. Cai et al. [85] have considered these factors and obtained thermal conductivity of suspended graphene as 2500 (+1000/-1050) W/m-K around 350 K. Studies on exfoliated graphene deposited on SiN_x [94] or silicon dioxide [95] revealed that thermal conductivity of three-layer samples is 1250 W/m-K while single-layer samples is 600 W/m-K.

Apart from investigations on thermal conductivity of pristine graphene, various factors such as isotopic doping [96], vacancy [97,98], surface functionalization [99], edge configurations [100,101], size effect [102–104] and strain [105,106] have also been explored. The effects of these factors originate from different scattering mechanisms, which operate over distinct frequency ranges and thus lead to different impacts on thermal transport. For example, mass disorder and vacancy primarily scatter high frequency phonons, whereas low-frequency phonons are less affected by these point defects. In contrast, boundary scattering can suppress low frequency phonons to a great extent. In real-world structures, multiple scattering mechanisms often coexist. For instance, in a graphene nanoribbon with mass disorder, thermal conductivity is governed by both boundary and point defect scattering. The boundary scattering can suppress the high frequency phonons [107], while the point defects are able to cause a weak phonon localization effect.

The material *h*-BN has boron and nitrogen atoms adjacent to carbon in the periodic table, resulting in some similarities to carbon-based materials. Compared with graphene and other 2D materials, monolayer *h*-BN exhibits exceptionally high chemical stability. Interest in 2D *h*-BN initially arose because bulk *h*-BN crystals [108] serve as outstanding substrates for graphene, enhancing its electronic properties by nearly an order of magnitude [109]. Like graphene, *h*-BN can exist in single layer, bilayer, and multilayer forms. However, in contrast to graphene, experimental data associated with few-layer *h*-BN's thermal conductivity remain relatively scarce. The thermal conductivity of suspended bilayer *h*-BN has been obtained by performing PDMS-assisted dry-transfer process, yielding a value of approximately 484 W/m-K at 300 K [110]. This value exceeds that of bulk *h*-BN [111] but remains lower than the predicted value for monolayer *h*-BN [112], demonstrating a clear thickness dependence of thermal conductivity of *h*-BN [113]. Moreover, by employing an innovative suspended micro-bridge device equipped with U-shaped resistance thermometers, the thermal conductivities of multilayer mechanically exfoliated *h*-BN can be measured [87]. The results show that the thermal conductivity of 11-layer *h*-BN and 5-layer *h*-BN is 360 W/m-K and 227∼280 W/m-K, respectively. The lower thermal conductivity observed in thinner samples is attributed to polymer residue on the h-BN surface [87].

Before the discovery of graphene, TMDs have already existed. Following graphene's demonstration of excellent properties, TMDs have regained the attention of researchers. TMDs typically have the form MX_2, where M is a transition metal and X is a chalcogen. Due to their tunable and diverse nature, these materials exhibit a wide range of excellent properties, in some aspects exceeding those of graphene. Among TMDs, MoS_2 has garnered tremendous interest due to its potential applications in electronic and optoelectronic devices [114,115]. Notably, its band gap is strongly dependent on layer number. For example, in bulk form, MoS_2 possesses an indirect band gap of 1.3 eV. In monolayer form, MoS_2 has a direct gap of 1.8 eV [116]. Similar to graphene and *h*-BN, TMDs can exist in monolayer, bilayer, and multilayer forms. The thermal conductivity of supported monolayer MoS_2 has been reported to be 62 W/m-K [117]. However, another study has exfoliated monolayer MoS_2 from bulk material, and analyzed its temperature-dependent Raman spectra, reporting a thermal conductivity in the range of 30.5∼38.5 W/m-K [118]. Sahoo et al. [89] has synthesized multilayer MoS_2 using chemical vapor deposition method and measured its thermal conductivity. Their results indicate that the thermal conductivity of an 11-layer MoS_2 is approximately 52 W/m-K at 300 K. The effect of thickness on the thermal conductivity of MoS_2 has also been investigated. Experimental results indicate that, the thermal conductivity decreases with increasing thickness. The reason can be clarified in this way: with the increase of thickness, the group velocity decreases and phonon scattering rate increases, which lead to the reduce of thermal conductivity [119]. WS_2 is another representative TMD. Due to its structural similarity to MoS_2, its thermal conductivity is expected to be comparable [118]. This has been verified by using optothermal Raman technique, which reports a thermal conductivity of 32 W/m-K for WS_2 [120]. The slight thermal conductivity difference between WS_2 and MoS_2 originates from the different phonon frequency variation due to distinct atomic masses of W and Mo. Furthermore, for multilayer WSe_2 with disordered stacking, a remarkably low cross-plane thermal conductivity of 0.05 W/m-K has been measured using TDTR [121].

After the successful synthesis of monolayer black phosphorus (BP) in 2014, it attracted renewed attention in the field of 2D materials. Unlike graphene, phosphorene possesses a puckered lattice structure, in which phosphorus atoms are arranged in an anisotropic configuration, giving rise to distinct armchair and zigzag directions. This structural feature originates from out-of-plane puckering, which breaks in-plane symmetry and leads to pronounced anisotropic properties [122]. Moreover, the electronic properties of phosphorene are both layer-dependent [123, 124] and edge dependent [125]. Phosphorene exhibits unique thermal transport behavior compared with other 2D materials such as graphene or TMDs. For example, Ong et al. studied the thermal transport in single-layer phosphorene using first-principles calculations and the non-equilibrium Green's function method, and showed that the thermal conductance along zigzag directions is approximately 40% higher than along armchair direction at 300 K [126]. Furthermore, strain can effectively modulate thermal transport anisotropy. Uniaxial tensile strain applied along zigzag direction enhances the thermal conductance in that direction, whereas strain applied along the armchair direction reduces the thermal conductance along the zigzag direction. This pronounced orientation-dependent thermal transport behavior has also been verified by MD simulation [127,128], first-principle calculations [129,130].

Overall, the thermal conductivity of 2D materials is governed not only by intrinsic lattice properties but also by dimensionality, defects, interfaces, and external perturbations. These factors provide versatile routes for phonon engineering while simultaneously posing challenges for quantitatively predicting thermal transport in realistic devices.

2.2.2.2. Thermal properties characterization of 2D materials. To understand the microscopic origin of the thermal conductivity discussed above, accurate characterization techniques are indispensable. Recent advances in ultrafast optical and electrical measurements have therefore played a crucial role in revealing phonon transport mechanisms in 2D materials.

Accurate characterization of thermal transport in 2D materials requires experimental techniques capable of probing heat transfer across ultrafast temporal and nanoscale spatial scales. Existing methods (the summary table comparing these experimental methods is shown in Table 1) can generally be divided into optical-based and electrical-based techniques. Optical methods, including TDTR [140], Raman thermometry [132], and thermoreflectance thermal imaging (TTI) [147], employ optical heating and detection to investigate thermal conductivity and interfacial heat transport. TDTR provides high temporal resolution and sensitivity, but typically requires a metallic transducer layer. Raman thermometry is noncontact and suitable for atomically thin materials, although its accuracy depends on reliable optical absorption calibration. TTI enables multi-timescale thermal imaging and simultaneous extraction of multiple thermal parameters, while its spatial resolution is limited by LED-based heating. In contrast, electrical-based methods such as the suspended micro-bridge technique directly measure intrinsic

Table 1
Comparison of thermal characterization techniques.

Technique	Category	Principle	Spatial Resolution	Temperature Resolution	Measured Quantity	Mapping Capability	Typical Applications	Main Limitation
SThM [131]	Temperature Mapping	Probe-sample heat exchange	20-100 nm	0.01-0.1 K	T, local κ, local q	Yes (Scanning)	Nanoscale hotspots	Tip-induced thermal resistance and slow scanning
Raman [132] Thermometry	Temperature Mapping	Temperature-dependent Raman peak shift	0.5 μm	1-5 K	T	Yes (Scanning)	2D materials, GaN, HEMT, SiC MOSFETs	Low temperature sensitivity
Transient Raman Thermometry [16, 133]	Temperature Mapping/Property characterization	Time-resolved Raman response under pulsed heating	0.5 μm	1 K	T, κ, alpha	Yes (Scanning)	Graphene, MoS_2, h-BN, Nanowire	Required pulsed laser system
Thermoreflectance Imaging [134–136]	Temperature Mapping	Temperature-dependent reflectivity variation	0.2-0.5 μm	0.2 K	T	Yes (Full-field)	CPU/GPU/HBM, hotspot mapping	Reflectivity calibration required
Time-Resolved TR Imaging [137]	Temperature Mapping	Ultrafast full-field thermorefectance imaging	0.2-0.5 μm	0.1 K	T, transient thermal response	Yes (Full-field)	HBM, transient hotspot evolution	High instrumentation complexity
3 Ω Method [138, 139]	Thermal Property Characterization	Third-harmonic thermal response from periodic Joule heating	0.1-10 μm	0.01 K	κ, G/TBC	No	Thin film, TIM, dielectric layer	Requires microfabricated heaters
TDTR [140,141]	Thermal Property Characterization	Pump-probe thermoreflectance	1 μm	0.2 K	κ, G/TBC, Cp	No	Interfaces, TIM, Advanced packaging	Femtosecond laser
FDTR [140,142]	Thermal Property Characterization	Frequency-domain thermoreflectance	1 μm	0.1-0.2 K	κ, alpha, G/TBC	No	Multilayer structures	Complex thermal modeling
T-type [143]	MEMS Thermal Bridge	Suspended sample attached to heater forming T geometry	100 nm	—	κ	No	Nanowires, CNTs, polymer fibers	Complex device fabrication
H-type [144,145]	MEMS Thermal Bridge	Dual suspended islands connected by sample	100 nm	—	κ,G	No	Graphene, MoS_2, 2D materials	Alignment and fabrication challenges
Suspended Thermal Bridge [83,146]	MEMS Thermal Bridge	Direct heat-flow measurement across suspended sample	100 nm	—	κ,G/TBC	No	Graphene, *h*-BN, vdW materials	MEMS fabrication required

thermal transport through Joule heating and electrical thermometry, but require complex device fabrication. Benefiting from their complementary advantages, these techniques have greatly advanced the understanding of phonon transport in 2D materials.

In TDTR measurements [147], as illustrated in Fig. 5 (a), the laser pulse generated by a Ti:sapphire laser is divided into pump and probe beams. The pump beam is intensity-modulated to periodically heat the sample surface, while the probe beam detects the surface temperature oscillation after a controlled delay time introduced by an electrically driven stage. The thermal response phase as a function of delay time can then be obtained. In a typical R_{TDTR} measurement, shown in Fig. 5 (b), the laser spot position is precisely controlled to achieve high-spatial-resolution mapping of thermal resistance. Fig. 5 (c) presents the R_{TDTR} map and statistical analysis for the heterobilayer with twist angle $\theta = 50°$. The thermal resistance of the heterobilayer region (R_0) was determined by Gaussian fitting of the histogram distribution, and the measurement uncertainty was quantified by the standard deviation of the fitted peak. Using the dual-wavelength flash Raman method, as illustrated in Fig. 5 (d), Zhang et al. [16] measured the thermal conductivity of suspended and supported monolayer WS_2 over 200–400 K. In this technique, one pulsed laser was used to heat the sample, while another pulsed laser monitored the transient temperature rise through Raman spectroscopy. By varying the delay time between the two laser pulses, the complete transient temperature evolution within one heating cycle could be reconstructed. Prior to the thermal conductivity measurements, the relationship between temperature and Raman peak shift was calibrated under 532 nm excitation over 100–500 K, as shown in Fig. 5 (e). This calibration enabled accurate temperature extraction and ensured that the temperature rise remained below 50 K, allowing radiative heat loss to be neglected. The thermal conductivity was then obtained by fitting the normalized transient temperature curves, as shown in Fig. 5 (f). In addition, Fig. 5 (g) shows that the E^1_{2g} (Γ) mode exhibits a blue shift in supported WS_2, suggesting that substrate coupling enhances the restoring force of the in-plane vibrational mode and modifies the phonon dispersion relation. Using suspended micro-bridge method, Sheng et al. [15] have achieved reversible manipulation of phonon transport in a monolayer $MoSe_2$-WSe_2 heterojunction by modulating phonon thermal conductivity through the switching of bias voltage. As illustrated in Fig. 5 (h), two gold sensors were employed simultaneously as heaters and thermometers. A large current was applied to one sensor to heat the sample, while a smaller current was used in the other sensor to monitor the resulting temperature rise. The thermal conductivity was then extracted by fitting the measured temperature signals with finite-element simulations of heat conduction. Fig. 5 (i) presents the SEM image of the monolayer $MoSe_2$-WSe_2 lateral heterostructure, and Fig. 5 (j) shows the thermal conductivity variation under different bias voltages. Liu et al. [148] have proposed a multi-pulse TTI combining with structure function algorithm, achieving simultaneous measurement of the thermal conductivities, specific heat capacities, and TBRs of microscale heterostructures. As illustrated in Fig. 5 (k), the testing system employed an LED to heat the sample surface and a detector to collect the reflected signal. To achieve an approximately ideal step response, a signal generator with a rise time of 20–100 ns was used. To enable measurements over a broad time range, a multi-pulse heating strategy was adopted, as shown in Fig. 5 (l). The early-stage thermal response was measured using short heating pulses, while the later-stage response was obtained using long heating pulses. By combining multiple datasets, a high-temporal-resolution transient thermal response spanning from tens of nanoseconds to hundreds of milliseconds was achieved. Fig. 5 (m) presents the transient temperature rise measured by TTI.

Although significant progress has been achieved in thermal characterization, rare experimental technique can simultaneously achieve ultrahigh spatial resolution, ultrafast temporal resolution, and comprehensive thermal-property extraction. Future advances are expected to integrate complementary characterization techniques with data-driven analysis to enable more accurate measurements of phonon

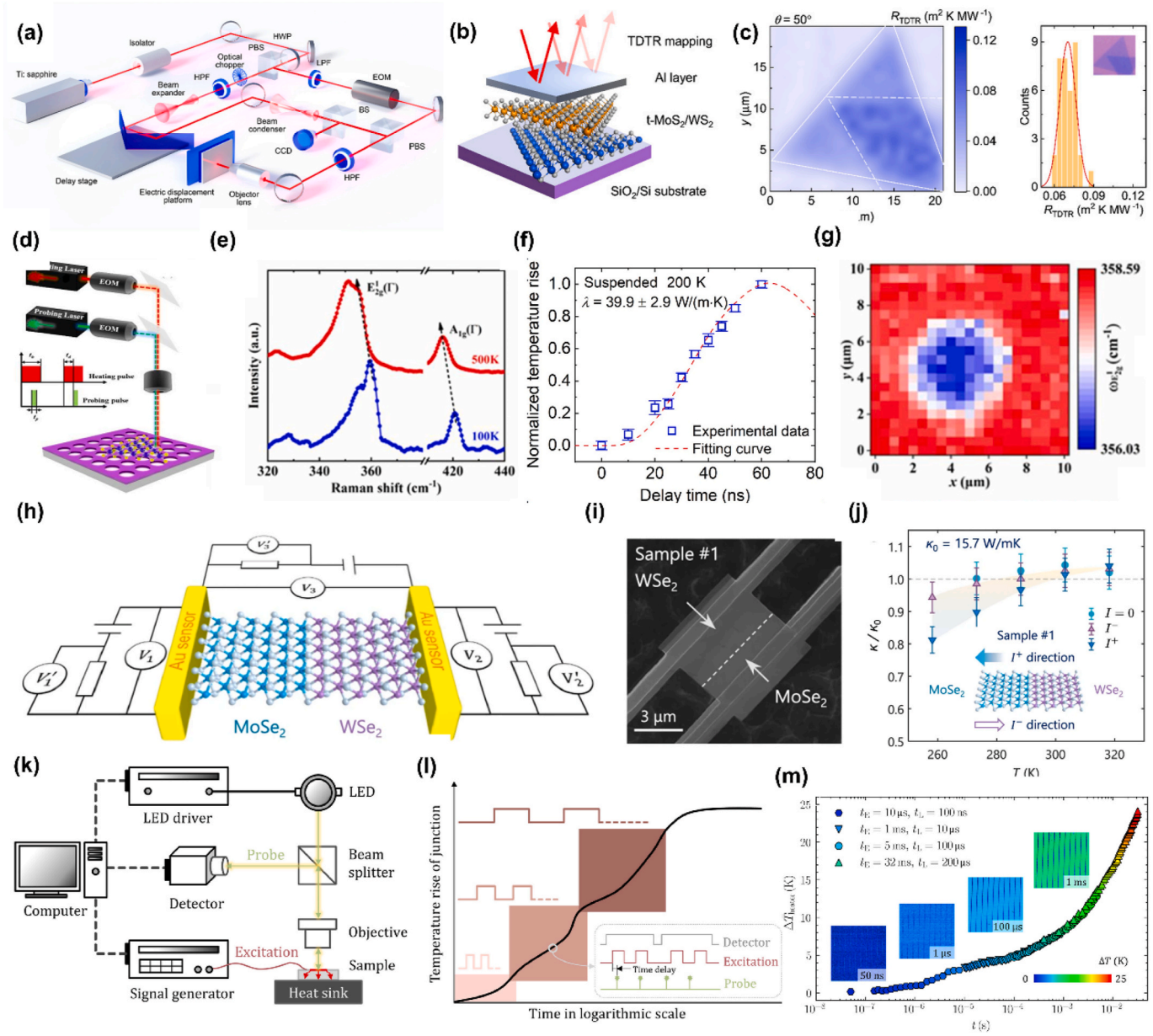

Fig. 5. Experimental measurement method of thermal properties for 2D materials (a-c) Time domain thermal reflectance method for twisted MoS_2/WS_2 heterostructure [147], (d-g) Dual-wavelength flash Raman method for measuring the thermal conductivity of monolayer WS_2 [16], (h-j) Suspended micro-bridge method for thermal conductivity measurement of 2D lateral heterostructure [15], (k-m) Multi-pulse TTI for achieving simultaneous measurement of the thermal conductivities, specific heat capacities, and thermal boundary resistances (TBRs) of microscale heterostructures [148].

transport.

While thermal conductivity measurements provide macroscopic transport properties, they cannot directly reveal the underlying transport mechanisms. Recent theoretical and experimental studies have therefore shifted from measuring thermal conductivity to identifying collective phonon transport phenomena, including hydrodynamic transport and coherent phonon transport.

Phonon hydrodynamics has recently emerged as an important topic in the study of thermal transport in 2D materials, providing a collective transport picture beyond the conventional particle-like phonon diffusion framework. Analogous to classical fluid hydrodynamics, phonon hydrodynamics describes the macroscopic collective motion of phonons when momentum-conserving normal (N) scattering processes dominate over momentum-destroying resistive (R) processes, such as Umklapp and defect scattering. Under such conditions, phonons can establish local equilibrium through frequent N scattering, leading to fluid-like heat transport phenomena, including second sound and phonon Poiseuille flow. The concept of second sound, originally proposed in superfluid helium as a wave-like propagation of thermal energy, has since been extended to crystalline solids and is regarded as one of the most representative signatures of hydrodynamic phonon transport. According to Peierls' theory, thermal transport in solids can evolve through different regimes with decreasing temperature, including kinetic, Ziman hydrodynamic, Poiseuille hydrodynamic, and ballistic regimes, depending on the competition among Umklapp scattering, normal scattering, and boundary scattering. In recent years, low dimensional materials with reduced phase space for Umklapp scattering and exceptionally long phonon mean free paths have provided an ideal platform for observing phonon hydrodynamic behaviors. Particularly in 2D materials, the unique phonon dispersion and strong normal scattering open new opportunities for realizing hydrodynamic heat transport even beyond conventional cryogenic conditions.

Using density-functional perturbation theory and an exact solution of the Boltzmann transport equation, Cepellotti et al. [149]. Revealed that momentum-conserving N scattering dominates over U scattering in several 2D materials, including graphene, h-BN, MoS_2, graphene, and fluorographene, over a wide temperature range extending up to room temperature, as shown in Fig. 6 (a). Unlike conventional three-dimensional solids, this unusual scattering hierarchy enables hydrodynamic phonon transport regimes, such as Poiseuille and Ziman flow, as well as wave-like heat propagation (second sound) in graphene, h-BN, and graphene. In graphene ribbons, dominant N scattering facilitates collective phonon flow and enhances thermal conductivity beyond the ballistic limit, as shown in Fig. 6 (b). As temperature increases, the system gradually evolves from the Poiseuille regime to the Ziman hydrodynamic regime, while the conventional kinetic regime dominated by Umklapp scattering is largely absent in these 2D materials. Using a microscale experimental platform in Fig. 6 (c) combined with first-principles-based kinetic theory, researchers experimentally demonstrated phonon Poiseuille flow in suspended isotopically purified graphite ribbons with a width of 5.5 μm up to 90 K [150]. In the hydrodynamic regime, collective phonon motion gives rise to a parabolic heat-flux profile, analogous to viscous fluid flow in confined channels. The thermal transport properties were measured using a μ-TDTR pump–probe technique on graphite ribbons with different widths. Conventional identification based on the temperature dependence of $\kappa/T^{2.5}$ was found insufficient to distinguish hydrodynamic transport from ballistic transport, especially in narrow ribbons in Fig. 6 (d). Therefore, the ratio of thermal conductivity to ballistic thermal conductance ($\kappa/G_{ballistic}$) was proposed as a more reliable criterion. For the 1.3 μm-wide ribbon, $\kappa/G_{ballistic}$ decreases monotonically with temperature, indicating a transition from ballistic to diffusive transport in Fig. 6 (e). In contrast, wider ribbons exhibit signatures of phonon Poiseuille flow, providing strong evidence for hydrodynamic phonon transport in graphite.

Using a phonon hydrodynamics strategy, researchers [151] realized directional heat transport rectification in isotopically enriched graphite by designing a micrometer-scale Tesla valve structure within a 90 nm-thick graphite crystal in Fig. 6 (f). Thermal transport measurements revealed a clear directional dependence of thermal conductivity, with a maximum thermal diodicity of 15.2% observed at 45 K in Fig. 6 (g). The temperature-dependent thermal diodicity shows that below

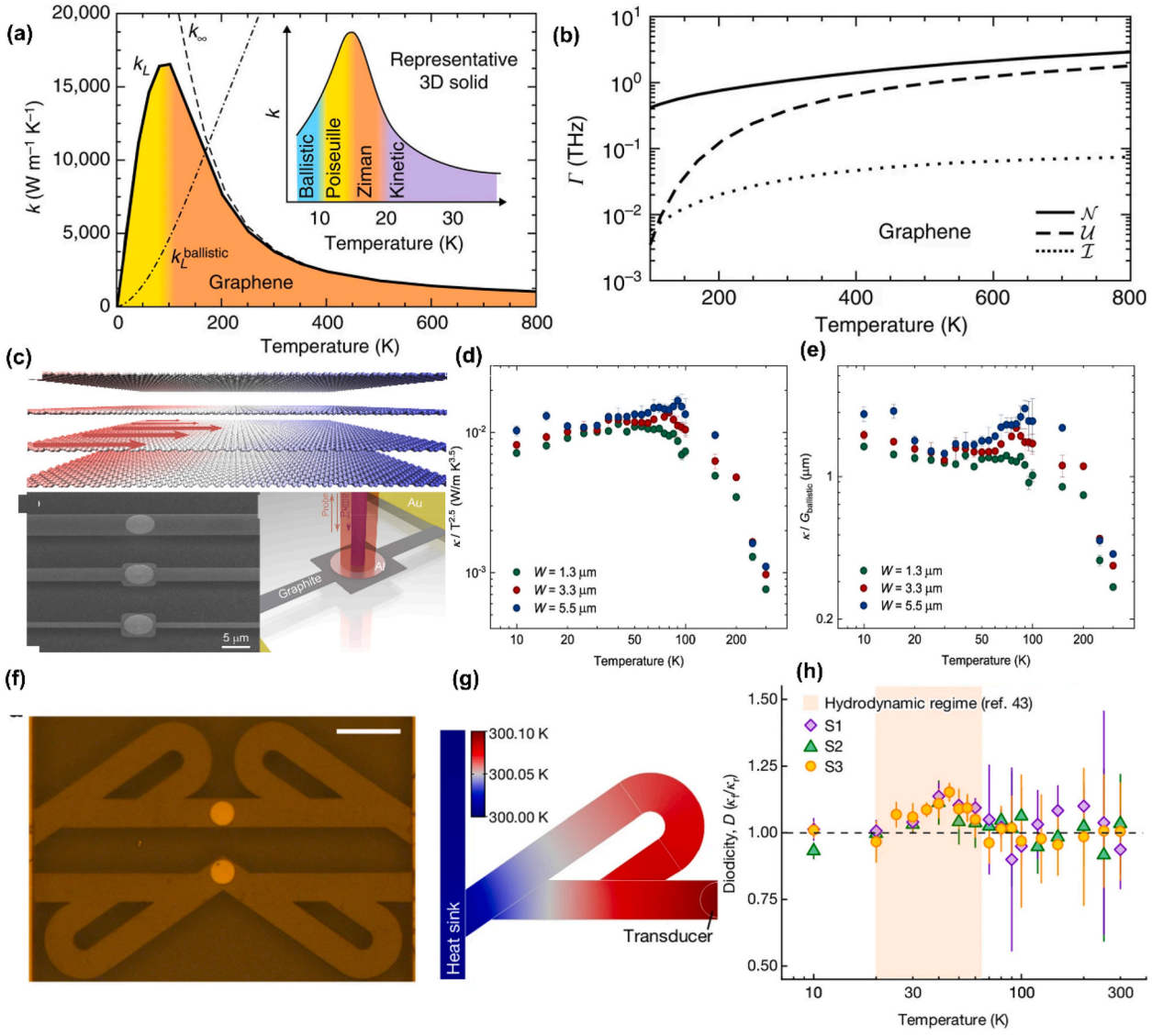

Fig. 6. Phonon hydrodynamics in 2D materials (a) Thermal transport regimes in two- and three-dimensional (3D) materials, (b) Average linewidths of normal (N), Umklapp (U) and isotopic (I) scattering processes in infinite suspended sheets of graphene [149], (c) Illustration of phonon Poiseuille flow in graphite ribbon, (d-e) The ratio of thermal conductivity over $T^{2.5}$ as a function of temperature for graphite ribbons with various widths and the ratio of thermal conductivity over $G_{ballistic}$ as a function of temperature [150], (f-h) A graphite thermal Tesla valve driven by hydrodynamic phonon transport [151].

20 K the ratio between forward and reverse thermal conductivity remains close to unity, indicating symmetric ballistic phonon transport. As temperature increases, momentum-conserving normal (N) scattering becomes dominant, enabling collective phonon flow characteristic of the hydrodynamic regime. Around 45 K, phonon hydrodynamic fluxes are established within the asymmetric Tesla valve channels while resistive Umklapp scattering remains weak in Fig. 6 (h). Owing to the geometric asymmetry of the Tesla valve, phonons propagate more efficiently in the forward direction, whereas stronger resistance is induced in the reverse direction, leading to higher forward thermal conductivity. This work demonstrates the potential of exploiting collective phonon hydrodynamics for thermal rectification and advanced thermal management in microscale and nanoscale devices.

2.2.2.3. Collective phonon transport in 2D materials. Besides hydrodynamic phonon transport, another important manifestation of collective phonon behavior is coherent phonon transport, in which the wave nature and phase correlation of phonons play a significant role in heat conduction [152,153]. Unlike the conventional phonon gas model that treats phonons as independent particles, coherent transport arises from constructive or destructive interference between phonon wave packets and becomes particularly important in periodically structured materials, superlattices, and phononic metamaterials when the phonon coherence length is comparable to the characteristic structural dimensions.

Recent theoretical developments have considerably advanced the understanding of phonon coherence. Zhang et al. proposed a generalized heat conduction formalism that naturally incorporates both particle-like and wave-like phonon behaviors through coherence time and phonon lifetime, providing a unified framework beyond the conventional phonon gas model [53]. Furthermore, direct atomic simulations demonstrated that thermal phonons consist of ensembles of coherent elastic wave packets, leading to intrinsic and mutual coherence effects that moderately enhance phonon relaxation times and thermal conductivity [54]. More recently, an analytical framework incorporating spatial coherence was developed to accurately describe phonon transmission across multi-interface heterostructures. The study revealed that spatial coherence has little influence on a single interface but becomes essential for accurately predicting phonon transmission and wave-packet evolution in complex multilayer structures [154]. These advances suggest that coherent phonon transport represents another important collective transport regime and provides new opportunities for manipulating thermal transport through interface engineering and phononic metamaterial design.

Collectively, these studies demonstrate that phonon transport in low-dimensional materials extends well beyond the conventional diffusive picture. Future efforts should focus on bridging hydrodynamic transport, coherent transport, and nonequilibrium phonon dynamics to establish a unified framework for collective phonon transport.

2.2.2.4. Asymmetric thermal transport and thermal devices based on 2D materials. Beyond understanding collective phonon transport, increasing efforts have been devoted to exploiting these thermal transport mechanisms for thermal functional devices. Among them, asymmetric thermal transport has emerged as one of the most representative applications.

Asymmetric thermal transport, also known as thermal rectification [155,156], refer to the diode-like behavior of heat flux, in which the magnitude of heat flux depends on the direction of thermal transport. This phenomenon has attracted considerable attention because of its potential applications in thermal management, phononic devices, and energy-saving systems. Previous studies have demonstrated thermal rectification in various asymmetric nanoscale systems, including structures with asymmetric geometries [144,157,158], mass gradient [159], and porous or compositionally inhomogeneous materials [160,161]. In these systems, asymmetric heat transport generally originates from mechanism such as direction-dependent overlap of phonon spectra under reversed temperature gradients [162], asymmetric phonon ballistic transport and boundary phonon scattering [157,163], as well as the coupled dependence of thermal conductivity on both temperature and spatial position [164]. Compared with conventional bulk materials, 2D materials provide a unique platform for realizing asymmetric thermal transport due to their atomic-scale thickness, strong phonon sensitivity to interfacial coupling, and high flexibility in structural design. In particularly, the arbitrary stacking and assembly of different 2D materials enable the construction of diverse vdW heterostructures with tunable interfacial interactions and symmetry breaking [12,165]. These characteristics make 2D materials highly promising for investigating thermal rectification phenomena and developing next-generation nanoscale thermal devices.

For in-plane lateral heterostructures, asymmetric thermal transport has been experimentally demonstrated in monolayer $MoSe_2$-WSe_2 lateral heterostructure systems, as shown in Fig. 7 (a) [160]. Due to the intrinsic asymmetry of the lateral heterointerface and the mismatch of phonon transport across the junction, heat conduction from $MoSe_2$ to WSe_2 is significantly more efficient than that in the reverse direction, resulting in a thermal rectification factor approaching 96% under high-bias conditions in Fig. 7 (b). Furthermore, the rectification effect can be effectively tuned by varying the interface orientation angle, highlighting the important role of interfacial symmetry and phonon coupling in regulating directional heat transport. Besides lateral heterostructures, vertically stacked vdW heterostructures also exhibit remarkable asymmetric heat transport in the out-of-plane direction. A representative example is the trilayer MoS_2/MoSSe/WSe_2 vdW heterostructure in Fig. 7 (c) ~ (e), which achieves strong thermal rectification within an atomically thin structure of less than 5 nm [134]. By controlling the asymmetric stacking sequence and interfacial twist angles, the variation in interfacial thermal conductance under opposite temperature gradients can exceed 100% in Fig. 7 (g) ~ (h). The asymmetric heat transport behavior originates from the different contributions of in-plane and out-of-plane phonon modes at the heterointerfaces, while twist-angle engineering further regulates phonon coupling and interlayer heat transport. Meanwhile, one field-effect transistor (FET) device with a MoS_2/MoSSe/WSe_2 trilayer on top of two thin gold electrodes was fabricated and the surface temperature distribution of the device was measured by using a non-contact transient thermal image method. The average temperature rises above the heating electrode, as shown in Fig. 7 (i), demonstrated that it exhibited a favorable linear relationship with heating power, which originates from the asymmetry in interfacial thermal conductance. Both lateral and vertically stacked 2D heterostructures provide effective routes for achieving asymmetric thermal transport through interfacial and structural engineering [134,160,166].

In summary, significant progress has been made in realizing thermal rectification in 2D heterostructures. However, further improvements in room temperature rectification efficiency and large-scale integration of thermal devices remain essential for practical applications. Future advances in interface engineering, twist-angle engineering, and phononic metamaterials are expected to accelerate the development of programmable thermal-functional devices and broaden their applications in nanoscale thermal management and phononic computing.

2.2.3. Thermal properties of vdW heterostructures

Materials scientists often combine different materials to form heterojunctions, which can exhibit enhanced performance arising from synergistic interactions between their constituent components. Such heterojunctions integrate materials with distinct properties and may lead to performance exceeding the sum of individual contributions. A well-known example is the PN junction transistor, which revolutionized modern electronics. The PN junction is a heterojunction made of two different types of semiconductor materials. Heterojunctions have attracted significant research interest due to their unique physical phenomena. However, despite their advantages, their practical

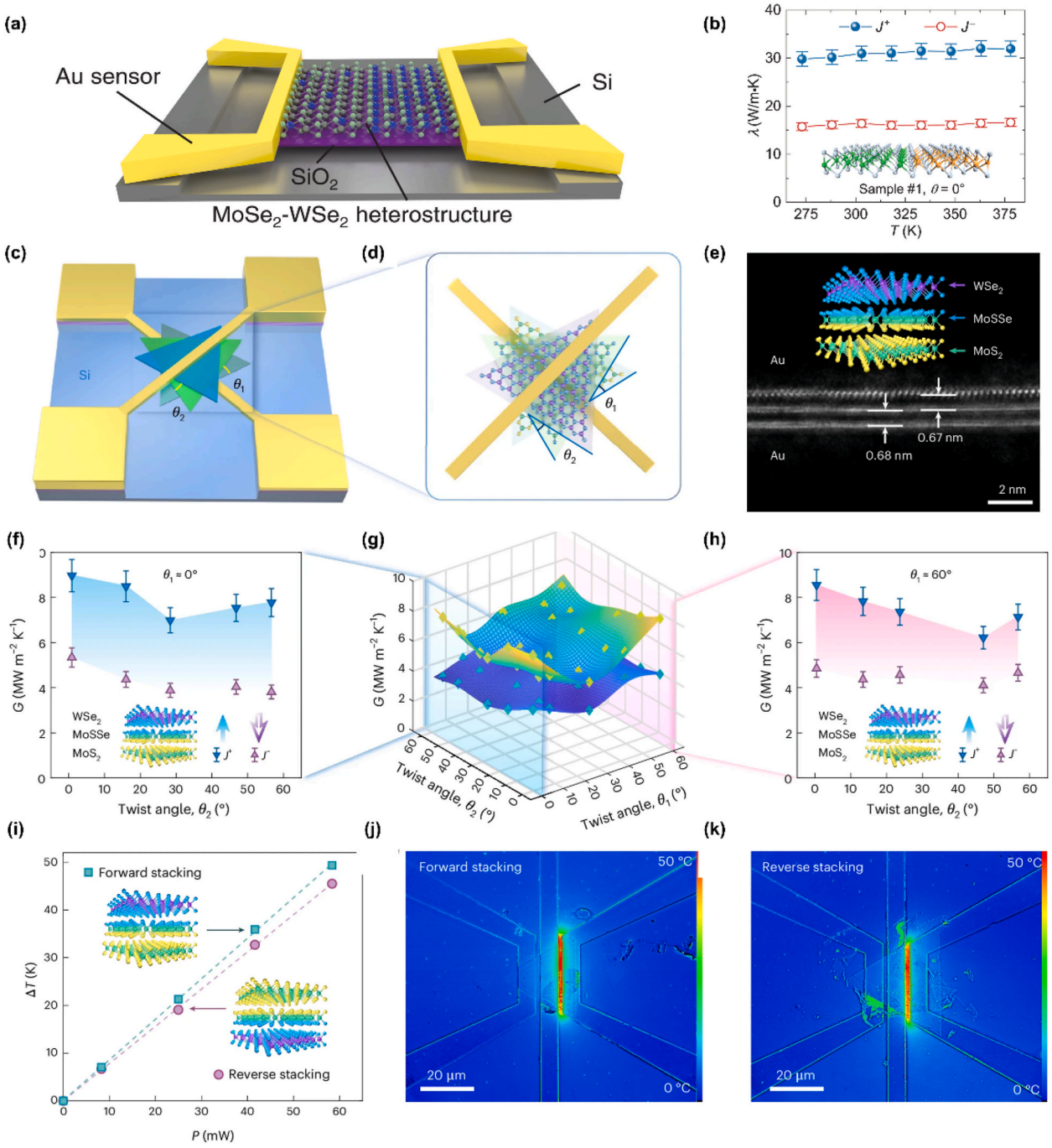

Fig. 7. Asymmetric thermal transport in 2D heterostructure (a-b) Thermal rectification across lateral $MoSe_2$/WSe_2 heterostructure [160], (c-d) Asymmetric thermal transport characterization across interlayer interface of multilayer heterostructure based on suspended micro-bridge measurement, (f-h) Asymmetric interlayer thermal conductance with twisted angle, (i-k) Asymmetric thermal transport in multilayer heterostructure device based on transient thermal image method [134].

realization remains challenging. When materials with significantly different lattice constants are combined, numerous defects can arise, degrading interfacial quality and device performance. A common strategy to address this issue is to introduce a buffer layer to accommodate films with different lattice constants. However, buffer layers may introduce additional interfacial defects and variability in thermal and electronic properties. As a result, high-quality heterojunctions are typically limited to materials with good lattice matching, which constrains the range of feasible material combinations.

Recently, with advances in micro-nano technologies, researchers have developed approaches to assemble 2D materials layer by layer, forming so-called vdW heterostructures. In these systems, strong covalent bonds ensure the in-plane stability of 2D crystals, while comparatively weak vdW forces are enough to hold the layers together in a stack. Unlike conventional heterostructures, lattice matching is no longer a strict requirement in vdW heterostructures, enabling the integration of dissimilar 2D materials through layer-by-layer stacking. This unique characteristic allows for the design of heterostructures with tailored functionalities by combing materials with diverse properties. The experimental demonstration of multilayer vdW heterostructures is a recent achievement [167–169]. Remarkably, these atomic-scale structures perform much better than anticipated. Additionally, the vertical stacking of 2D materials possessing various electronic, optical, and magnetic properties allows for the creation of a wide range of vdW

heterostructures. The varied characteristics of different heterostructures offer unparalleled possibilities for various applications [170]. Examples include vertical field-effect transistors (VFETs) (Fig. 8 (a) and (b)), ultrasensitive infrared photodetectors (Fig. 8 (c)), Light-Emitting Devices (LEDs) (Fig. 8 (d)), spin-filtering devices (Fig. 8 (e) and (f)), which are difficult to achieve in traditional material heterostructures.

Moreover, 2D materials possess a high surface-to-volume ratio, enabling interfacial properties to play a dominate role in the overall system design. Beyond materials composition in vdW heterostructures, stacking order [1,6,177], interlayer rotation [7,8] and cross-plane strain [11] have also been shown to be effective strategies for engineering thermal conductivity of vdW heterostructures. For example, Using a combinatorial experimental approach, Aditya et al. [177] have probed nine graphene-MoS_2 heterostructures constructed by distinct sequence, and identified an optimized superlattice with ultralow thermal conductivity comparable to that of air, as shown in Fig. 9 (a). The effect of rotation angle on interfacial thermal transport of graphene/*h*-BN heterostructures has been investigated by using MD simulation [7]. It was reported that the thermal conductance reaches as high as 509 MW/(m^2K) at 500 K in the absence of rotation, and as decreases monotonically with increasing rotation angle, as shown in Fig. 9 (b). The influence of cross plane strain has also been investigated [11], showing that thermal conductance can be tuned from 50% to 350% of its original value through modulating cross-plane strain, as illustrated in Fig. 9 (c).

Among various modulation strategies, interlayer twist offers a nondestructive and controllable approach to tailoring the physical behaviors of 2D vdW systems and uncovering emergent phenomena [178]. The relative rotation between adjacent layers introduces lattice mismatch and gives rise to moiré patterns, which can significantly modify interlayer coupling and reconstruct the phonon and electronic band structures. Analogous to twistronics in electronic systems, "twistonics" has recently emerged as a promising concept for manipulating phonon behaviors through interlayer twist engineering. By altering phonon dispersion, scattering processes, and interlayer interactions, twist engineering provides an effective route to regulate thermal transport in 2D materials. Consequently, increasing efforts have been devoted to exploring the twist-angle-dependent thermal transport properties of representative 2D vdW materials.

It has been reported that large-area vdW MoS_2 thin films with random interlayer rotations (r-MoS_2) exhibit ultralow thermal conductivities in the cross-plane direction (57 ± 3 mW $m^{-1}K^{-1}$), comparable to that of ambient air (~26 mW $m^{-1}K^{-1}$), as shown in Fig. 10 (a) and (b). Homogeneous non-equilibrium molecular dynamics (HNEMD) simulations suggest that this anomalously low thermal conductivity originates from the strong suppression of transverse acoustic (TA) modes and the overdamping of longitudinal acoustic (LA) modes, which together severely hinder heat transport along the cross-plane direction [8], as shown in Fig. 10 (c). In contrast to the conventional understanding of homogeneous materials, Zhang et al. [147] reported a significant enhancement of interfacial thermal conductance in twisted MoS_2/WS_2 heterostructures, as shown in Fig. 10 (d). This enhancement was attributed to efficient optical-to-acoustic phonon conversion through inelastic scattering, which introduces additional transport channels that compensate for the intrinsic phonon mismatch at the heterogenous interface. Hu et al. [179] further investigated the twist-angle dependence of thermal transport in Gr/*h*-BN bilayer heterostructures. The simulation setup is illustrated in Fig. 10 (f). As shown in Fig. 10 (g), the thermal conductivity exhibits a pronounced nonmonotonic dependence

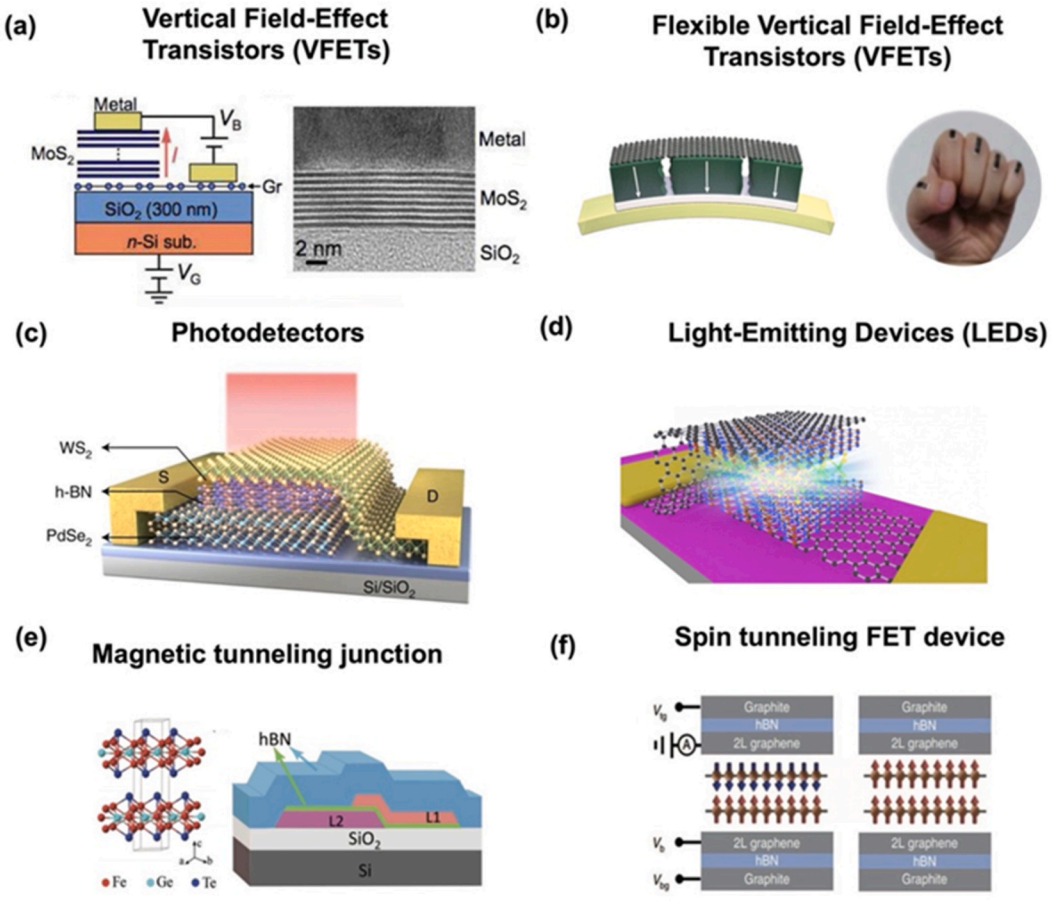

Fig. 8. Applications of 2D vdW heterostructures. (a) VFETs [171], (b) Flexible VFETs [172], (c) Photodetectors [173], (d) LEDs [174], (e) Magnetic tunneling junction [175] and (f) Spin tunneling FET device [176].

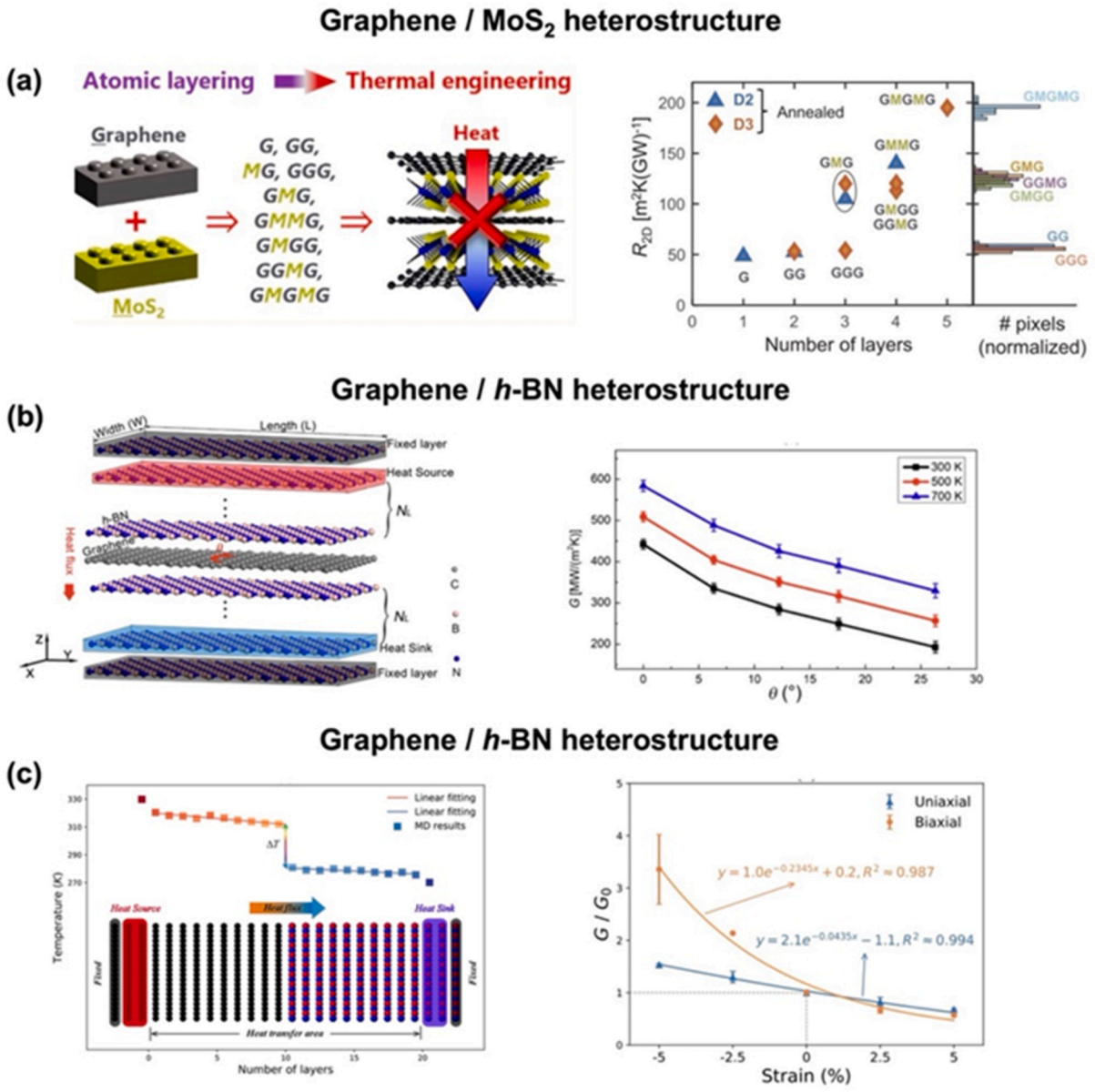

Fig. 9. Strategies for engineering phonon transport: (a) stacking order [177], (b) interlayer rotation [7] and (c) cross-plane strain [11].

on twist angle, reaching a maximum at 17.9°, where the conductivity is enhanced by approximately 125% compared with the untwisted AA-stacked structure. This anomalous enhancement was attributed to enhanced in-plane basal phonon transport resulting from weakened interlayer coupling and suppressed anharmonicity at intermediate twist angles. Although these studies establish twist engineering as an effective strategy for tailoring phonon transport, the underlying microscopic mode-resolved phonon transport mechanisms remain insufficiently understood. To address this issue, Ding et al. [23] investigated interlayer thermal transport in twisted graphene using mode-resolved atomistic Green's function. The thermal conductance was found to strongly dependence on rotation angle, with the highest value at 0° and the lowest at 10°. Mode-analysis further revealed that twisting particularly suppresses high-frequency phonons with large incidence angles, as shown in Fig. 10 (h).

Taken together, these studies demonstrate a paradigm shift in thermal transport engineering of vdW heterostructures, from conventional material selection toward interface engineering. Stacking sequence, twist angle, and strain provide complementary approaches for reconstructing phonon dispersion, tuning interlayer coupling, and regulating phonon scattering. Among them, twist engineering has emerged as one of the most powerful and versatile strategies because it enables reversible and nondestructive control of phonon transport without modifying chemical composition. Nevertheless, several fundamental challenges remain. The microscopic origin of twist-dependent phonon transport is still under debate, and the reported twist-angle dependences often vary among different material systems due to differences in interface quality, transport regime, and theoretical methodology. Moreover, the enormous design space generated by diverse 2D materials, stacking configurations, twist angles, and external stimuli remains largely unexplored. Future advances are expected to integrate first-principles calculations, machine-learning-assisted high-throughput screening, and advanced thermal characterization techniques to establish universal structure-phonon transport relationships and accelerate the rational design of thermal-functional vdW heterostructures.

Looking forward, the combination of twist engineering, strain engineering, external electric fields, and machine-learning-guided inverse design is expected to enable programmable thermal transport in vdW

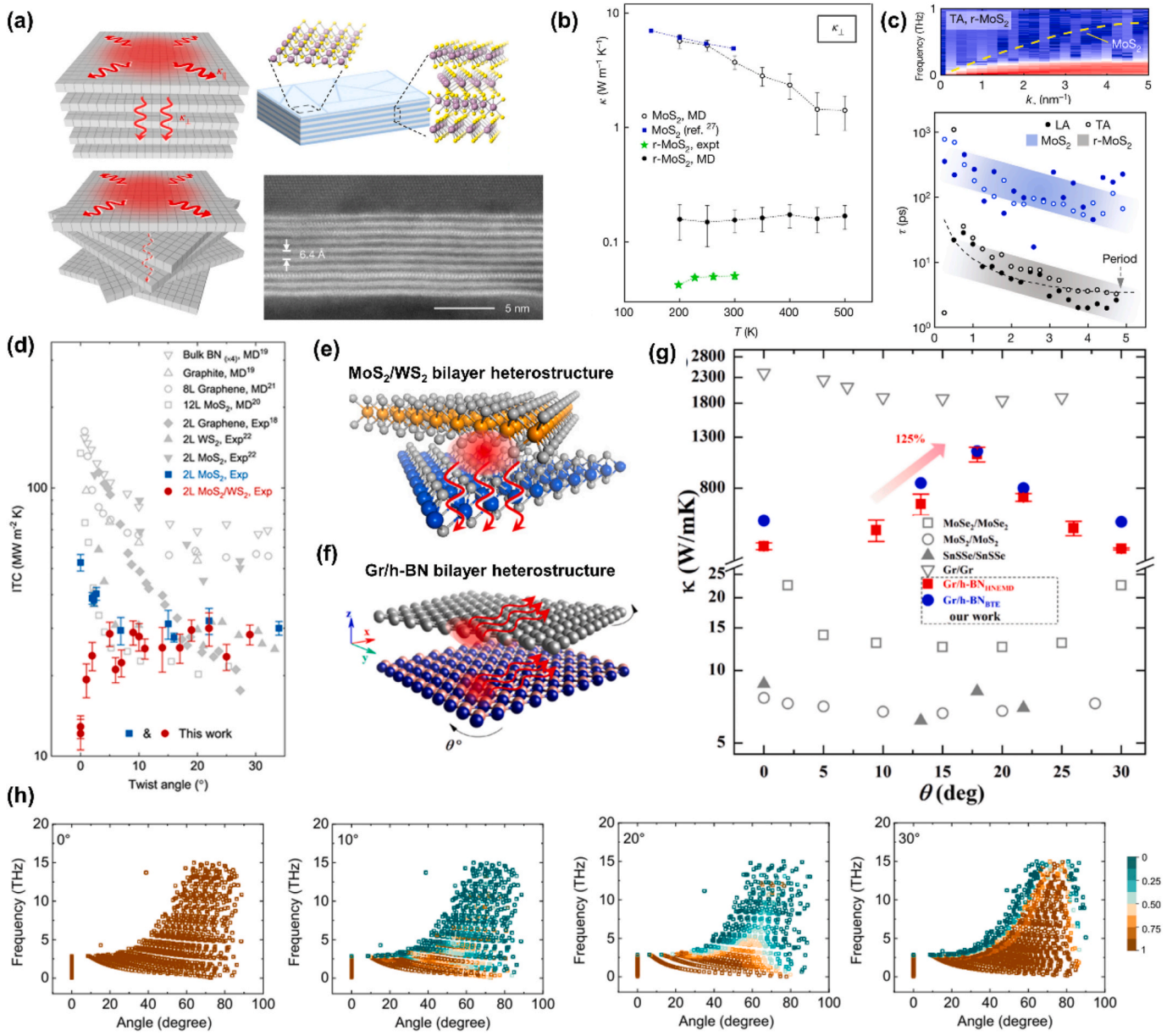

Fig. 10. Twisting-induced thermal conductivity modulation and phonon transport mechanism. (a) Schematic of an r-MoS_2 film with random crystalline orientation, and HAADF-STEM image of a cross-section of an $N = 10$ r-MoS_2 film on AlOx coated with Al, with an interlayer spacing of 6.4 Å, (b) Experiment and MD simulation results of κ(T) of MoS_2 and r-MoS_2 films [8], (c) TA phonon dispersion curves of r-MoS_2 along the Γ-A direction. The dotted lines denote the acoustic curves corresponding to bulk MoS_2, and lifetime of LA and TA phonons parallel to the Γ-A direction in bulk and r-MoS_2. The dashed line is the LA mode vibration period derived from the dispersion curve [8], (d) The interlayer interfacial thermal conductance across various twisted 2D homo/heterostructure materials [147], (e) The atomic configuration of twisted MoS_2/WS_2 [147], (f) The atomic configuration of twisted graphene/h-BN [179], (g) Room-temperature lattice thermal conductivity of twisted Gr/h-BN, computed using both HNEMD and BTE methods [179], (h) Mode-resolved phonon transport in twisted graphene [179].

heterostructures. Such developments may facilitate the realization of next-generation phononic devices, thermal logic circuits, and intelligent thermal management systems.

2.3. MI for vdW heterostructures

MI offers a revolutionary approach to accelerate the discovery of materials with targeted properties. By integrating simulations or experimental data with ML techniques, MI enables the exploration of complex, multiscale relationships that are difficult to capture using traditional approaches. ML encompasses several learning paradigms, including supervised, unsupervised, semi-supervised, and reinforcement learning [180]. In supervised learning, the dataset includes features referred to as the independent variables and a target or dependent variable. In contrast, unsupervised learning lacks a target variable. Semi-supervised learning involves training data where only some examples have target labels. In reinforcement learning, the model is trained on data with minimal labeling, but it uses a system of rewards and penalties based on the algorithm's output. ML methods are widely applied to tasks such as classification, regression, clustering, and optimization, as illustrated in Fig. 11. Classification and regression are predictive tasks, where the former aims to predict a discrete class label and the latter predicts a continuous value. Clustering algorithms group data points into clusters based on similarity, maximizing intra-cluster properties and minimizing inter-cluster differences. In addition, optimization techniques, including evolutionary algorithms such as genetic

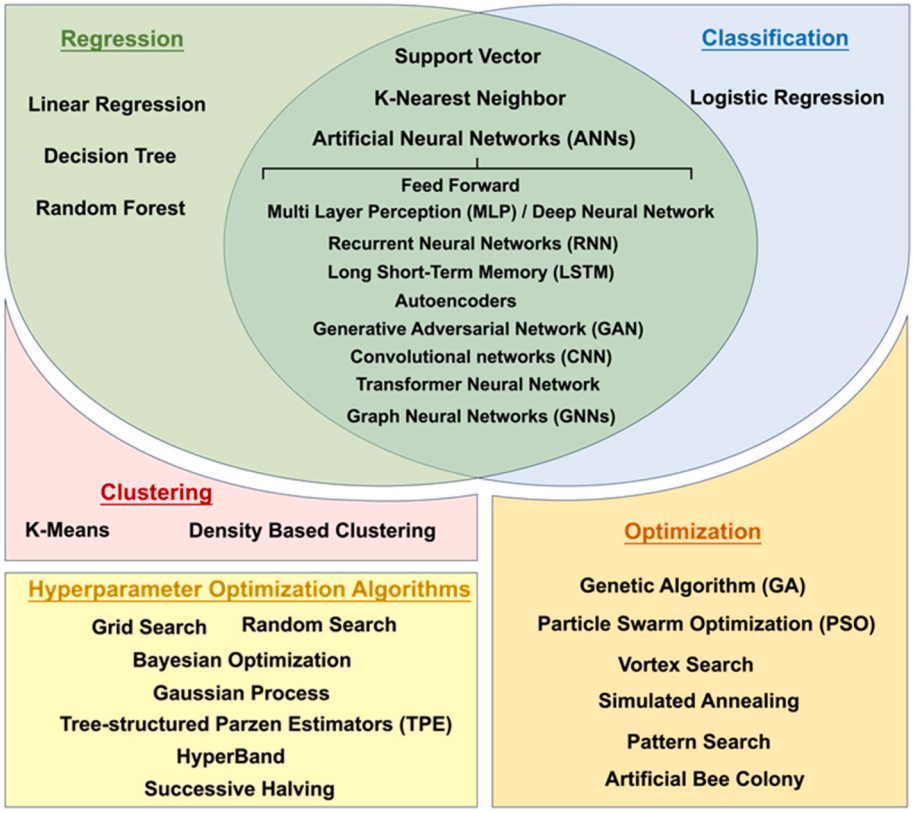

Fig. 11. ML methods.

algorithms and particle swarm optimization. Hyperparameter tuning aims to improve a ML model's effectiveness by finding optimal settings for its hyperparameters. These methods provide a foundation for modeling complex relationships in materials systems.

The core of materials science relates is processing-structure-property-performance relationships. As illustrated in Fig. 12, this framework exhibits a many-to-one relationship from processing to performance, indicating that different processing routes may lead to similar material performance, and a one-to-many relationship from properties to structure, implying that a given property can arise from multiple underlying structures. In this framework, the left-to-right mapping corresponds a forward problem, where material properties are predicted from processing and structure, typically formulated as data-driven model. For example, to predict properties of vdW heterostructures, a forward model has been constructed through 2D material dataset, theoretical calculations, and supervised ML methods [181] as shown in Fig. 13 (a). In contrast, the right-of-left mapping corresponds to an inverse problem, aiming to identify or design material with desired properties. This inverse design problem is often formulated as an optimization task. For instance, an artificial neural network model has been

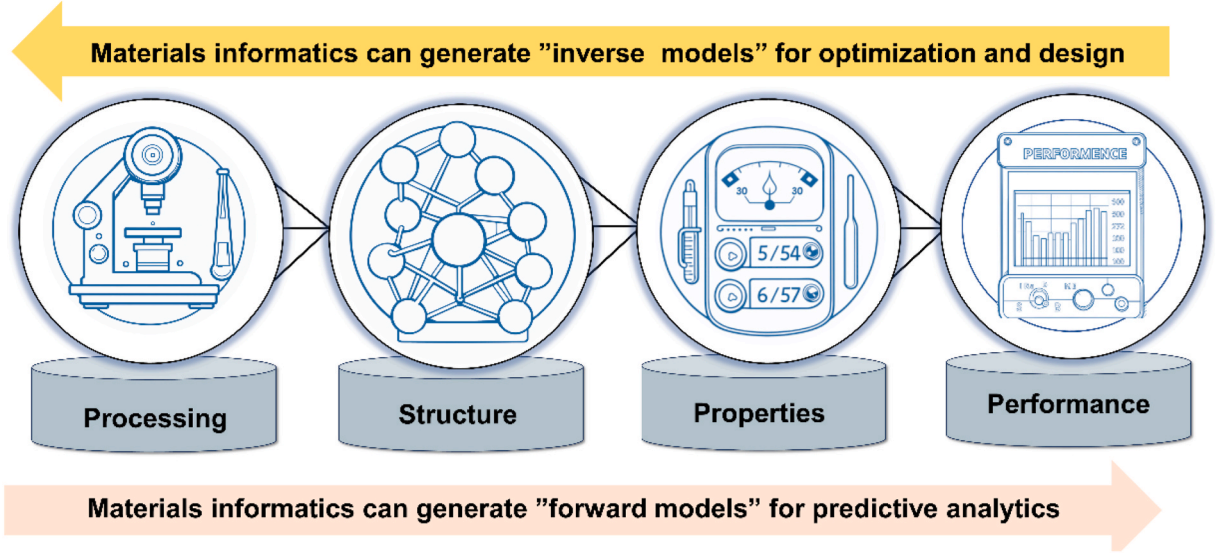

Fig. 12. The relationships between processing, structure, property, and performance in materials science and engineering, along with the role of MI in unraveling these connections through both forward and inverse modeling approaches.

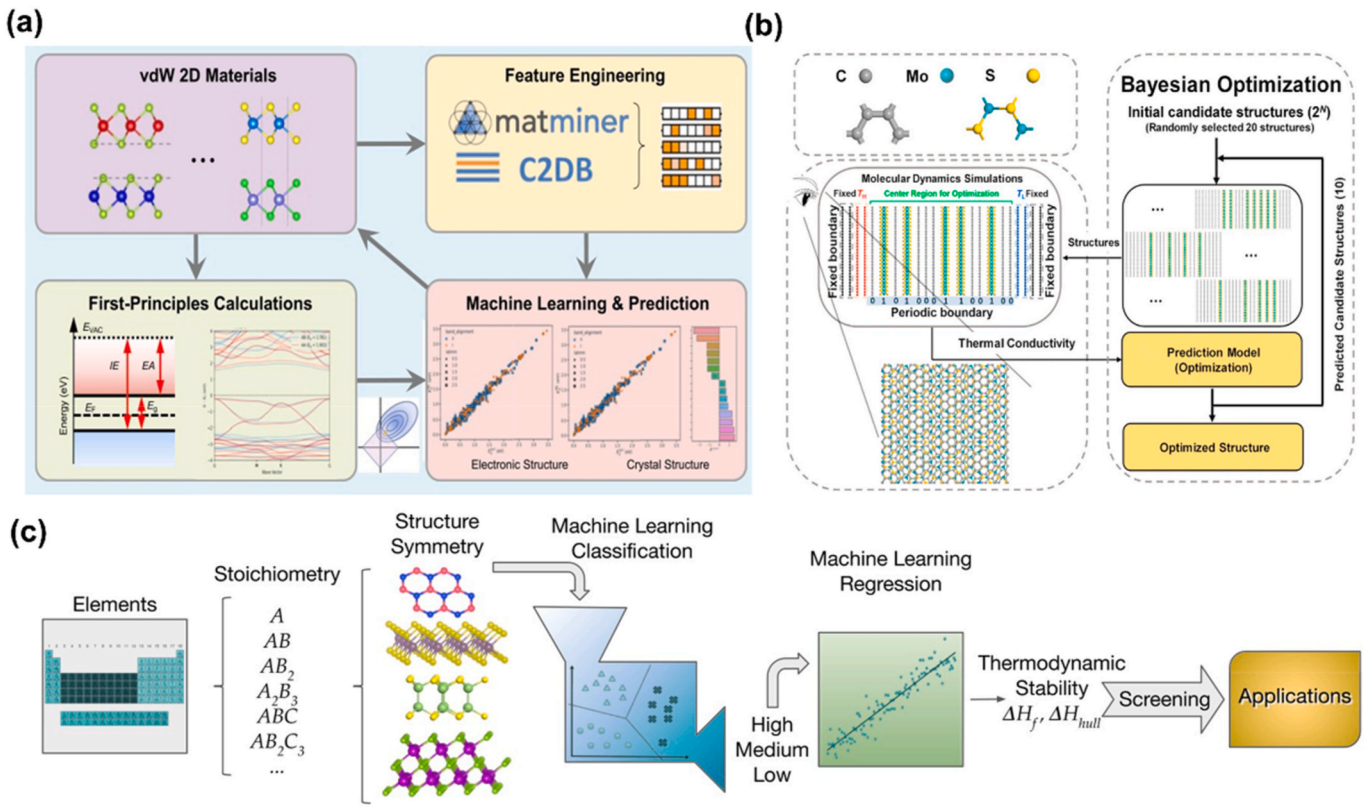

Fig. 13. ML in vdW heterostructures. (a) Schematics of combining the MD and Bayesian optimization [181], (b) Schematic of combining the MD and Bayesian optimization [1], and (c) schematic of data-driven process to discover and design materials [182].

constructed and employed to identify eight types of 2D materials with an accuracy exceeding 90% [183]. By combining Bayesian optimization with NEMD simulations, Hu et al. [1] achieved an optimized graphene-MoS_2 heterostructure exhibiting ultralow thermal conductivity approaching to that of air, as shown in Fig. 13 (b). In addition, ML-based approaches can also be used to extract physically meaningful descriptors. Gabriel et al. [182] have demonstrated that descriptors derived from formation energy and convex hull data in the C2DB 2D materials database can effectively classify materials within specific structural families, as shown in Fig. 13 (c).

In addition, recent advances in data-driven materials research have enabled not only the discovery of structures with extreme thermal properties but also the development of systematic phonon regulation strategies, as illustrated in Fig. 14. Ding et al. [165] introduced a human-AI collaborative framework to study heat conduction in 2D vdW heterostructures. In this work, a self-learning entropic population annealing method combined with mode-resolved AGF calculations was employed to construct a globally representative and nearly complete thermal conductivity dataset over the entire configurational space. Such a comprehensive dataset enables analysis beyond localized phonon scattering mechanisms, allowing for full-spectrum phonon regulation, in which phonon transport is selectively suppressed across a broad range of phonon frequency and incidence angles. Using this dataset, ultralow thermal conductivity configurations on the order of 0.02 W/m-K were identified. Furthermore, physically interpretable descriptors were extracted to elucidate how specific stacking sequences govern frequency- and angle-dependent phonon transmission. By coupling ultralow thermal conductivity design with a complete and interpretable dataset, this work highlights a general strategy for full-spectrum phonon engineering and provides a valuable foundation for uncovering universal thermal transport in low-dimensional materials.

3. Conclusions and future perspectives

In summary, research on microscale and nanoscale thermal transport has significantly advanced the understanding of heat conduction beyond the classical Fourier framework, revealing the critical roles of phonon scattering, dimensional confinement, interfacial coupling, and quantum effects in low-dimensional systems. The rapid development of advanced experimental characterization techniques and atomistic simulation methods has established a comprehensive framework for probing and interpreting thermal transport phenomena in 2D materials and vdW heterostructures. Representative 2D materials, including graphene, *h*-BN, transition metal dichalcogenides, and black phosphorus, exhibit highly tunable thermal transport behaviors arising from their unique phonon dispersions, anisotropic structures, and strong sensitivity to defects, strain, stacking order, and interlayer interactions. Furthermore, vdW heterostructures provide an unprecedented platform for engineering heat transport through twist-angle modulation, interfacial coupling, and structural asymmetry, enabling emerging phenomena such as phonon hydrodynamics, asymmetric thermal transport, and ultralow thermal conductivity. These capabilities establish vdW heterostructures as a representative class of thermal functional materials, whose thermal properties can be deliberately tailored through structural design.

Despite these advances, several important challenges remain. Current theoretical and experimental studies often focus on isolated scattering mechanisms or limited structural configurations, making it difficult to establish a unified understanding of full-spectrum phonon transport across complex multiscale systems. In particular, accurately correlating microscopic phonon behaviors with macroscopic thermal responses under realistic device conditions remains a major challenge. In addition, interfacial thermal resistance, non-equilibrium phonon dynamics, and coupled transport involving electrons, spins, and ions continue to limit the predictive design of next-generation thermal

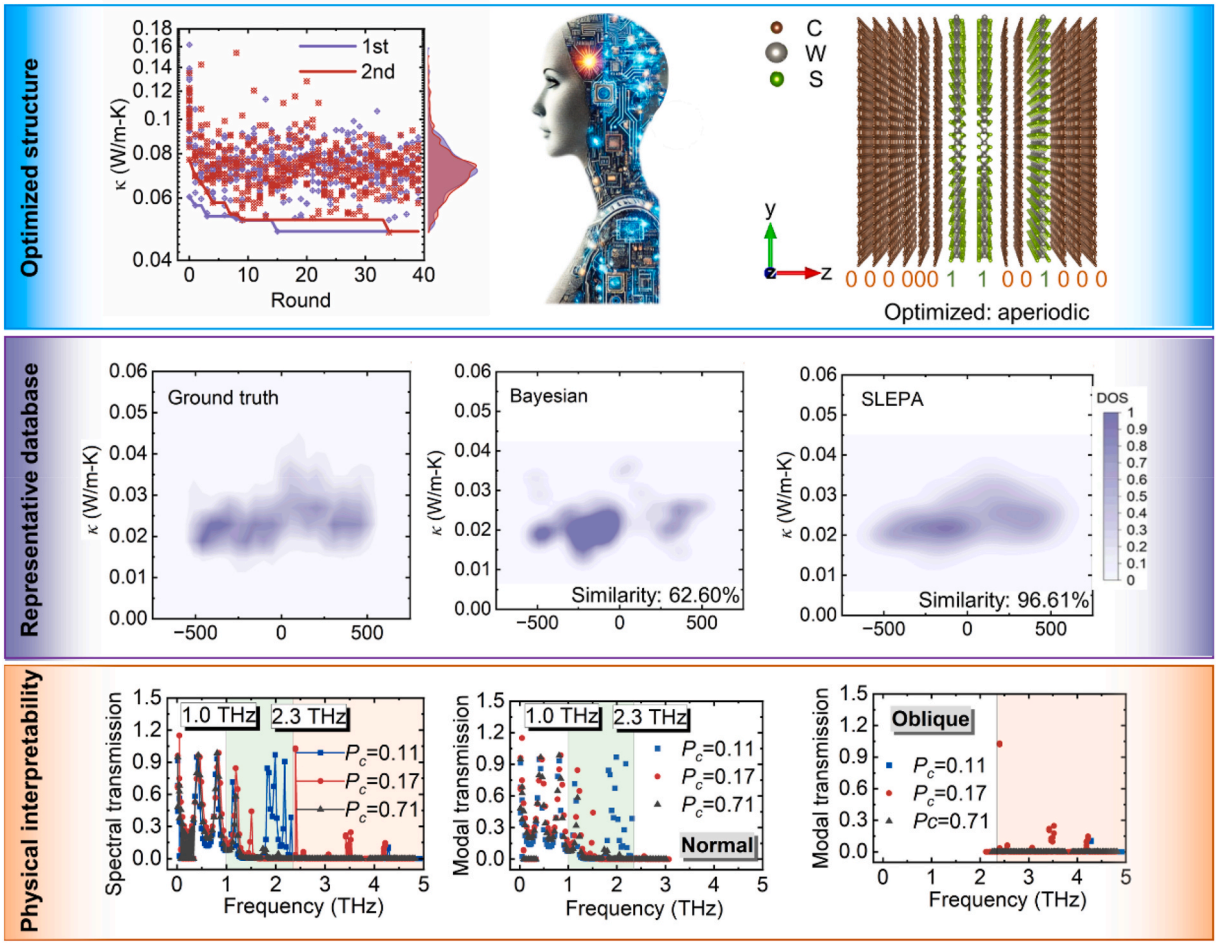

Fig. 14. The ML-driven paradigm for the design targeted thermal conductivity and understanding of heat conduction in 2D materials vdW heterostructures.

materials and devices. Future research is expected to increasingly combine advanced characterization, multiscale simulations, and MI to achieve predictive and physically interpretable thermal transport engineering. Data-driven approaches integrating ML with atomistic simulations and experimental datasets offer new opportunities for uncovering hidden structure-property relationships and accelerating the discovery of materials with tailored thermal functionalities. Particularly, the construction of comprehensive and representative thermal transport databases may enable the transition from case-by-case studies toward generalized and statistically robust design principles. At the same time, developing physically interpretable machine-learning frameworks will be essential for transforming data-driven models from purely predictive tools into platforms for mechanism discovery and phonon engineering.

Future progress in nanoscale thermal science will likely focus on several key directions. First, precise manipulation of interfacial thermal conductance is essential for reliable heat dissipation in highly integrated and heterogeneous electronic systems. Second, exploiting collective phonon behaviors, including hydrodynamic transport and coherent phonon effects, may provide new pathways for controlling heat flow beyond conventional diffusive limits. Third, low-dimensional materials with extreme thermal conductivities, strong anisotropy, and tunable interfacial coupling will continue to drive innovations in thermal management, thermoelectric energy conversion, and thermal devices. Finally, integrating *in situ* characterization, multiscale theoretical modeling, and physically informed data-driven methods will be crucial for translating fundamental phonon physics into scalable materials design strategies and practical technologies. Through the convergence of low-dimensional materials science, phonon engineering, and MI, nanoscale thermal transport research is expected to play an increasingly important role in next-generation electronics, sustainable energy systems, and emerging quantum and intelligent technologies.

CRediT authorship contribution statement

Wenyang Ding: Data curation, Formal analysis, Funding acquisition, Investigation, Methodology, Resources, Software, Validation, Visualization, Writing – original draft, Writing – review & editing. **Bingyang Cao:** Conceptualization, Data curation, Funding acquisition, Investigation, Project administration, Supervision, Validation, Visualization, Writing – original draft, Writing – review & editing.

Declaration of competing interest

The authors declare that they have no known competing financial interests or personal relationships that could have appeared to influence the work reported in this paper.

Acknowledgement

This study was financially supported by the National Natural Science Foundation of China (Grant Nos. 52506092, 52327809, 52425601, and 52250273), the China Postdoctoral Science Foundation (Grant Nos. 2025M770583, and 2026T190159), the Shuimu Tsinghua Scholar program of Tsinghua University, Beijing Natural Science Foundation (No. L233022), and National Key Research and Development Program of China (No. 2023YFB4404104).

References

[1] S. Hu, S. Ju, C. Shao, J. Guo, B. Xu, M. Ohnishi, J. Shiomi, Ultimate impedance of coherent heat conduction in van der Waals graphene-MoS_2 heterostructures, Mater. Today Phys. 16 (2021) 100324.

[2] J. Spiece, S. Sangtarash, M. Mucientes, A.J. Molina-Mendoza, K. Lulla, T. Mueller, O. Kolosov, H. Sadeghi, C. Evangeli, Low thermal conductivity in franckeite heterostructures, Nanoscale 14 (2022) 2593–2598.

[3] P.-Z. Jia, Y.-J. Zeng, D. Wu, H. Pan, X.-H. Cao, W.-X. Zhou, Z.-X. Xie, J.-X. Zhang, K.-Q. Chen, Excellent thermoelectric performance induced by interface effect in MoS_2/$MoSe_2$ van der Waals heterostructure, J. Phys. Condens. Matter 32 (2019) 055302.

[4] A. Liu, H. Xie, Z. Wu, Y. Wang, Advances and outlook of TE-PCM system: a review, Carbon Neutral 1 (2022) 20.

[5] T. Luo, G. Chen, Nanoscale heat transfer–from computation to experiment, Phys. Chem. Chem. Phys. 15 (2013) 3389–3412.

[6] R. Guo, Y.-D. Jho, A.J. Minnich, Coherent control of thermal phonon transport in van der Waals superlattices, Nanoscale 10 (2018) 14432–14440.

[7] W. Ren, Y. Ouyang, P. Jiang, C. Yu, J. He, J. Chen, The impact of interlayer rotation on thermal transport across graphene/hexagonal boron nitride van der Waals heterostructure, Nano Lett. 21 (2021) 2634–2641.

[8] S.E. Kim, F. Mujid, A. Rai, F. Eriksson, J. Suh, P. Poddar, A. Ray, C. Park, E. Fransson, Y. Zhong, D.A. Muller, P. Erhart, D.G. Cahill, J. Park, Extremely anisotropic van der Waals thermal conductors, Nature 597 (2021) 660–665.

[9] W. Ren, S. Lu, C. Yu, J. He, Z. Zhang, J. Chen, G. Zhang, Impact of moiré superlattice on atomic stress and thermal transport in van der Waals heterostructures, Appl. Phys. Rev. 10 (2023) 041404.

[10] T. Miao, J. Song, M. An, D. Chen, W. Ma, Interlayer coupling and twist-induced modulation of heat transport in multilayer β-bismuthene, Appl. Phys. Lett. 128 (2026) 112203.

[11] X. Wu, Q. Han, Phonon thermal transport across multilayer graphene/hexagonal boron nitride van der Waals heterostructures, ACS Appl. Mater. Interfaces 13 (2021) 32564–32578.

[12] W. Ding, Z.-Y. Ong, M. An, B. Davier, S. Hu, M. Ohnishi, J. Shiomi, Optimally Suppressed Phonon Tunneling in van der Waals Graphene–WS_2 Heterostructure with Ultralow Thermal Conductivity, Nano Lett. 24 (2024) 13754–13759.

[13] D.G. Cahill, Thermal conductivity measurement from 30 to 750 K: the 3ω method, Rev. Sci. Instrum. 61 (1990) 802–808.

[14] D.G. Cahill, Analysis of heat flow in layered structures for time-domain thermoreflectance, Rev. Sci. Instrum. 75 (2004) 5119–5122.

[15] Y. Sheng, H. Zhu, S. Xie, Q. Lv, H. Xie, H. Wang, R. Lv, H. Bao, Electrically-driven reversible phonon transport manipulation in two-dimensional heterostructures, Nat. Commun. 16 (2025) 1970.

[16] Y. Zhang, Q. Lv, A. Fan, L. Yu, H. Wang, W. Ma, R. Lv, X. Zhang, Reduction in thermal conductivity of monolayer WS_2 caused by substrate effect, Nano Res. 15 (2022) 9578–9587.

[17] S. Feng, H. Chen, J. Zhang, M. An, G. Zhang, Data-driven prediction of thermal conductivity from short MD trajectories: a GCN-LSTM approach, Chin. Phys. Lett. 43 (2026) 020801.

[18] D. Frenkel, B. Smit, Understanding Molecular Simulation: from Algorithms to Applications, Academic Press San Diego, 2002.

[19] J. Zhang, Y. Zhang, Z. Zhao, M. An, G. Zhang, Physical origin of high lattice thermal conductivity in β-Si_3N_4: a machine learning potential study, Rev. Mater. Res. 2 (2026) 100164.

[20] Z. Chen, Y. Yuan, Y. Wang, P. Ying, S. Li, C. Shao, W. Ding, G. Zhang, M. An, Softening of vibrational modes and anharmonicity induced thermal conductivity reduction in a-Si:H at high temperatures, Adv. Electron. Mater. (2025) 2500104 n/a.

[21] Z. Chen, Y. Yuan, W. Ding, S. Li, M. An, G. Zhang, Hyperparameter optimization and force error correction of neuroevolution potential for predicting thermal conductivity of wurtzite GaN, Chin. Phys. B 34 (2025) 086110.

[22] Y. Han, C. Yang, X. Cheng, D. Han, W. Ding, X. Wang, Investigation of the effect of four-phonon scattering on thermal transport in two-dimensional group-IV materials, ACS Appl. Energy Mater. 7 (2024) 649–656.

[23] W. Ding, J. Shiomi, B. Cao, Mode-resolved phonon transport in twisted graphene, Chin. Phys. Lett. 43 (2026), 040801-040801.

[24] J. Howell, M.P. Mengüç, R. Siegel, Thermal Radiation Heat Transfer, 2015.

[25] T.L. Bergman, Fundamentals of Heat and Mass Transfer, John Wiley & Sons, 2011.

[26] F. Incropera, D. DeWitt, Fundamentals of Heat Transfer, Seconded, John Wiley, New York, 1985.

[27] C.J. Glassbrenner, G.A. Slack, Thermal conductivity of silicon and germanium from 3 K to the melting point, Phys. Rev. J. Arch. 134 (1964) A1058.

[28] S. Li, Q. Zheng, Y. Lv, X. Liu, X. Wang, P.Y. Huang, D.G. Cahill, B. Lv, High thermal conductivity in cubic boron arsenide crystals, Science 361 (2018) 579–581.

[29] L. Lindsay, D.A. Broido, T.L. Reinecke, First-principles determination of ultrahigh thermal conductivity of boron arsenide: a competitor for diamond? Phys. Rev. Lett. 111 (2013) 025901.

[30] J.S. Kang, M. Li, H. Wu, H. Nguyen, Y. Hu, Experimental observation of high thermal conductivity in boron arsenide, Science 361 (2018) 575–578.

[31] F. Tian, B. Song, X. Chen, N.K. Ravichandran, Y. Lv, K. Chen, S. Sullivan, J. Kim, Y. Zhou, T.H. Liu, M. Goni, Z. Ding, J. Sun, G.A.G. Udalamatta Gamage, H. Sun, H. Ziyaee, S. Huyan, L. Deng, J. Zhou, A.J. Schmidt, S. Chen, C.W. Chu, P. Y. Huang, D. Broido, L. Shi, G. Chen, Z. Ren, Unusual high thermal conductivity in boron arsenide bulk crystals, Science 361 (2018) 582–585.

[32] S. Patankar, Numerical Heat Transfer and Fluid Flow, Taylor & Francis, 2018.

[33] A. Bejan, Convection Heat Transfer, John wiley & sons, 2013.

[34] T.M. Tritt, Thermal Conductivity: Theory, Properties, and Applications, Springer Science & Business Media, 2005.

[35] C. Kittel, P. McEuen, Introduction to Solid State Physics, John Wiley & Sons, 2018.

[36] A.A. Balandin, Thermal properties of graphene and nanostructured carbon materials, Nat. Mater. 10 (2011) 569–581.

[37] E. Pop, D. Mann, Q. Wang, K. Goodson, H. Dai, Thermal conductance of an individual single-wall carbon nanotube above room temperature, Nano Lett. 6 (2006) 96–100.

[38] A.A. Balandin, S. Ghosh, W. Bao, I. Calizo, D. Teweldebrhan, F. Miao, C.N. Lau, Superior thermal conductivity of single-layer graphene, Nano Lett. 8 (2008) 902–907.

[39] C. Chiritescu, D.G. Cahill, N. Nguyen, D. Johnson, A. Bodapati, P. Keblinski, P. Zschack, Ultralow thermal conductivity in disordered, layered WSe_2 crystals, Science 315 (2007) 351–353.

[40] J. Yang, B. Zhang, A.D. Christodoulides, Q. Xu, A. Zangiabadi, S.R. Peurifoy, C. K. McGinn, L. Dai, E. Meirzadeh, X. Roy, Solution-processable superatomic thin-films, J. Am. Chem. Soc. 141 (2019) 10967–10971.

[41] J.C. Duda, P.E. Hopkins, Y. Shen, M.C. Gupta, Exceptionally low thermal conductivities of films of the fullerene derivative PCBM, Phys. Rev. Lett. 110 (2013) 015902.

[42] X. Wang, C.D. Liman, N.D. Treat, M.L. Chabinyc, D.G. Cahill, Ultralow thermal conductivity of fullerene derivatives, Phys. Rev. B 88 (2013) 075310.

[43] A. Maznev, O. Wright, Demystifying umklapp vs normal scattering in lattice thermal conductivity, Am. J. Phys. 82 (2014) 1062–1066.

[44] D. Chen, H. Chen, S. Hu, H. Guo, S.W. Sharshir, M. An, W. Ma, X. Zhang, Influence of atomic-scale defect on thermal conductivity of single-layer MoS_2 sheet, J. Alloys Compd. 831 (2020) 154875.

[45] D. Han, W. Ding, X. Wang, L. Cheng, Tunable thermal transport in a WS_2 monolayer with isotopic doping and fractal structure, Nanoscale 11 (2019) 19763–19771.

[46] D. Han, X. Wang, W. Ding, Y. Chen, J. Zhang, G. Xin, L. Cheng, Phonon thermal conduction in a graphene–C_3N heterobilayer using molecular dynamics simulations, Nanotechnology 30 (2018) 075403.

[47] M. An, D. Chen, W. Ma, S. Hu, X. Zhang, Directly visualizing the crossover from incoherent to coherent phonons in two-dimensional periodic MoS_2/$MoSe_2$ arrayed heterostructure, Int. J. Heat Mass Transf. 178 (2021) 121630.

[48] W. Zhang, S. Xiong, Y. Guo, H.-L. Yi, M. Nomura, S. Volz, Promoting anderson localization for low-frequency phonons in SiGe alloyed nanowires with long-range correlated disorder, ACS Nano 19 (2025) 37004–37012.

[49] Y. Quan, S. Yue, B. Liao, Impact of electron-phonon interaction on thermal transport: a review, nanoscale microscale thermophys, Eng. 25 (2021) 73–90.

[50] X. Li, S. Lee, Crossover of ballistic, hydrodynamic, and diffusive phonon transport in suspended graphene, Phys. Rev. B 99 (2019) 085202.

[51] X. Sun, S. Lu, S. Shan, Z. Zhang, J. Chen, Origin of superdiffusive thermal transport in one-dimensional van der Waals atomic chains, Phys. Rev. B 111 (2025) 205404.

[52] C. Yu, S. Shan, S. Lu, Z. Zhang, J. Chen, Characteristics of distinct thermal transport behaviors in single-layer and multilayer graphene, Phys. Rev. B 107 (2023) 165424.

[53] Z. Zhang, Y. Guo, M. Bescond, J. Chen, M. Nomura, S. Volz, Heat conduction theory including phonon coherence, Phys. Rev. Lett. 128 (2022) 015901.

[54] Z. Zhang, Y. Guo, M. Bescond, J. Chen, M. Nomura, S. Volz, Generalized decay law for particlelike and wavelike thermal phonons, Phys. Rev. B 103 (2021) 184307.

[55] S. Lu, Z. Zhang, Y. Li, P. Hänggi, J. Chen, Single phonon diode operating on a metagrating surface, Phys. Rev. B 112 (2025) 075407.

[56] R.J. Stevens, L.V. Zhigilei, P.M. Norris, Effects of temperature and disorder on thermal boundary conductance at solid–solid interfaces: nonequilibrium molecular dynamics simulations, Int. J. Heat Mass Transf. 50 (2007) 3977–3989.

[57] L. Qiu, X. Zhang, Z. Guo, Q. Li, Interfacial heat transport in nano-carbon assemblies, Carbon 178 (2021) 391–412.

[58] J. Yang, Z. Lu, J. Wang, H. Liu, H. Li, J. Li, Y. Lu, Designs for low-thermal-resistance thermal interface materials: oriented high-conductivity networks, ultra-thin bond lines thickness and contact-resistance minimization, Adv. Nanocompos. 3 (2026) 133–148.

[59] Z. Tian, K. Esfarjani, G. Chen, Enhancing phonon transmission across a Si/Ge interface by atomic roughness: first-principles study with the Green's function method, Phys. Rev. B 86 (2012) 235304.

[60] Y. Liu, C. Hu, J. Huang, B.G. Sumpter, R. Qiao, Tuning interfacial thermal conductance of graphene embedded in soft materials by vacancy defects, J. Chem. Phys. 142 (2015) 244703.

[61] P.K. Schelling, S.R. Phillpot, P. Keblinski, Kapitza conductance and phonon scattering at grain boundaries by simulation, J. Appl. Phys. 95 (2004) 6082–6091.

[62] M. Sakata, T. Hori, T. Oyake, J. Maire, M. Nomura, J. Shiomi, Tuning thermal conductance across sintered silicon interface by local nanostructures, Nano Energy 13 (2015) 601–608.

[63] K. Zheng, F. Sun, X. Tian, J. Zhu, Y. Ma, F. Wang, Tuning the interfacial thermal conductance between polystyrene and sapphire by controlling the interfacial adhesion, ACS Appl. Mater. Interfaces 7 (2015) 23644–23649.

[64] Y. Hong, L. Li, X.C. Zeng, J. Zhang, Tuning thermal contact conductance at graphene–copper interface via surface nanoengineering, Nanoscale 7 (2015) 6286–6294.

[65] X.W. Zhou, R.E. Jones, J.C. Duda, P.E. Hopkins, Molecular dynamics studies of material property effects on thermal boundary conductance, Phys. Chem. Chem. Phys. 15 (2013) 11078–11087.
[66] L. Pan, J. Carrete, Z. Wang, G.K.H. Madsen, Machine learning boosted *ab initio* study of the thermal conductivity of Janus PtSTe van der Waals heterostructures, Phys. Rev. B 109 (2024) 035417.
[67] K.S. Novoselov, A.K. Geim, S.V. Morozov, D.-e. Jiang, Y. Zhang, S.V. Dubonos, I. V. Grigorieva, A.A. Firsov, Electric field effect in atomically thin carbon films, science 306 (2004) 666–669.
[68] A. Geim, K. Novoselov, Graphene calling, Nat. Mater. 6 (2007) 169.
[69] A.K. Geim, Graphene: status and prospects, science 324 (2009) 1530–1534.
[70] K. Novoselov, V. Fal, Ko, L. Colombo, P.R. Gellert, M.G. Schwab, K. Kim, Nature 490 (2012) 192–200.
[71] M. Salavati, A. Mojahedin, A. Shirazi, Mechanical responses of pristine and defective hexagonal boron-nitride nanosheets: a molecular dynamics investigation, Front. Struct. Civ. Eng. 14 (2020) 623–631.
[72] H. Du, X. Lin, Z. Xu, D. Chu, Recent development in Black phosphorus transistors, J. Mater. Chem. C 3 (2015) 8760–8775.
[73] T. Jiang, Q. He, M. bi, X. Chen, H. Sun, L. Tao, First-principles calculations of adsorption sensitivity of Au-doped MoS_2 gas sensor to main characteristic gases in oil, J. Mater. Sci. 56 (2021) 1–11.
[74] T.-f. Shi, J.-y. Zheng, X. Wang, P. Zhang, P.-a. Zong, K.M. Razeeb, Recent advances of electrodeposition of Bi_2Te_3 and its thermoelectric applications in miniaturized power generation and cooling, Int. Mater. Rev. 68 (2023) 521–555.
[75] T.V. Vu, H.D. Tong, T.K. Nguyen, C.V. Nguyen, A.A. Lavrentyev, O.Y. Khyzhun, B. V. Gabrelian, H.L. Luong, K.D. Pham, P.T. Dang, D.D. Vo, Enhancement of monolayer SnSe light absorption by strain engineering: a DFT calculation, Chem. Phys. 521 (2019) 5–13.
[76] V. Goyal, D. Teweldebrhan, A.A. Balandin, Mechanically-exfoliated stacks of thin films of Bi_2Te_3 topological insulators with enhanced thermoelectric performance, Appl. Phys. Lett. 97 (2010) 133117.
[77] H. Li, J. Wu, X. Huang, G. Lu, J. Yang, X. Lu, Q. Xiong, H. Zhang, Rapid and reliable thickness identification of two-dimensional nanosheets using optical microscopy, ACS Nano 7 (2013) 10344–10353.
[78] J. Zheng, H. Zhang, S. Dong, Y. Liu, C. Tai Nai, H. Suk Shin, H. Young Jeong, B. Liu, K. Ping Loh, High yield exfoliation of two-dimensional chalcogenides using sodium naphthalenide, Nat. Commun. 5 (2014) 2995.
[79] X. Huang, Z. Zeng, H. Zhang, Metal dichalcogenide nanosheets: preparation, properties and applications, Chem. Soc. Rev. 42 (2013) 1934–1946.
[80] X. Li, W. Cai, J. An, S. Kim, J. Nah, D. Yang, R. Piner, A. Velamakanni, I. Jung, I e. tutuc, sk banerjee, l colombo, rs ruoff, Science 324 (2009) 14.
[81] L. Song, L. Ci, H. Lu, P.B. Sorokin, C. Jin, J. Ni, A.G. Kvashnin, D.G. Kvashnin, J. Lou, B.I. Yakobson, Large scale growth and characterization of atomic hexagonal boron nitride layers, Nano Lett. 10 (2010) 3209–3215.
[82] S. Bae, H. Kim, Y. Lee, X. Xu, J.-S. Park, Y. Zheng, J. Balakrishnan, T. Lei, H. Ri Kim, Y.I. Song, Roll-to-roll production of 30-inch graphene films for transparent electrodes, Nat. Nanotechnol. 5 (2010) 574–578.
[83] X. Xu, L.F. Pereira, Y. Wang, J. Wu, K. Zhang, X. Zhao, S. Bae, C. Tinh Bui, R. Xie, J.T. Thong, Length-dependent thermal conductivity in suspended single-layer graphene, Nat. Commun. 5 (2014) 3689.
[84] S. Ghosh, W. Bao, D.L. Nika, S. Subrina, E.P. Pokatilov, C.N. Lau, A.A. Balandin, Dimensional crossover of thermal transport in few-layer graphene, Nat. Mater. 9 (2010) 555–558.
[85] W. Cai, A.L. Moore, Y. Zhu, X. Li, S. Chen, L. Shi, R.S. Ruoff, Thermal transport in suspended and supported monolayer graphene grown by chemical vapor deposition, Nano Lett. 10 (2010) 1645–1651.
[86] M.-H. Bae, Z. Li, Z. Aksamija, P.N. Martin, F. Xiong, Z.-Y. Ong, I. Knezevic, E. Pop, Ballistic to diffusive crossover of heat flow in graphene ribbons, Nat. Commun. 4 (2013) 1734.
[87] I. Jo, M.T. Pettes, J. Kim, K. Watanabe, T. Taniguchi, Z. Yao, L. Shi, Thermal conductivity and phonon transport in suspended few-layer hexagonal boron nitride, Nano Lett. 13 (2013) 550–554.
[88] H. Zhou, J. Zhu, Z. Liu, Z. Yan, X. Fan, J. Lin, G. Wang, Q. Yan, T. Yu, P. M. Ajayan, High thermal conductivity of suspended few-layer hexagonal boron nitride sheets, Nano Res. 7 (2014) 1232–1240.
[89] S. Sahoo, A.P. Gaur, M. Ahmadi, M.J.-F. Guinel, R.S. Katiyar, Temperature-dependent raman studies and thermal conductivity of few-layer MoS_2, J. Phys. Chem. C 117 (2013) 9042–9047.
[90] I. Jo, M.T. Pettes, E. Ou, W. Wu, L. Shi, Basal-plane thermal conductivity of few-layer molybdenum disulfide, Appl. Phys. Lett. 104 (2014) 201902.
[91] S. Lee, F. Yang, J. Suh, S. Yang, Y. Lee, G. Li, H. Sung Choe, A. Suslu, Y. Chen, C. Ko, Anisotropic in-plane thermal conductivity of Black phosphorus nanoribbons at temperatures higher than 100 K, Nat. Commun. 6 (2015) 1–7.
[92] Z. Luo, J. Maassen, Y. Deng, Y. Du, R.P. Garrelts, M.S. Lundstrom, P.D. Ye, X. Xu, Anisotropic in-plane thermal conductivity observed in few-layer Black phosphorus, Nat. Commun. 6 (2015) 8572.
[93] M.T. Pettes, J. Maassen, I. Jo, M.S. Lundstrom, L. Shi, Effects of surface band bending and scattering on thermoelectric transport in suspended bismuth telluride nanoplates, Nano Lett. 13 (2013) 5316–5322.
[94] Z. Wang, R. Xie, C.T. Bui, D. Liu, X. Ni, B. Li, J.T. Thong, Thermal transport in suspended and supported few-layer graphene, Nano Lett. 11 (2011) 113–118.
[95] J.H. Seol, I. Jo, A.L. Moore, L. Lindsay, Z.H. Aitken, M.T. Pettes, X. Li, Z. Yao, R. Huang, D. Broido, N. Mingo, R.S. Ruoff, L. Shi, Two-dimensional phonon transport in supported graphene, Science 328 (2010) 213–216.
[96] S. Chen, Q. Wu, C. Mishra, J. Kang, H. Zhang, K. Cho, W. Cai, A.A. Balandin, R. S. Ruoff, Thermal conductivity of isotopically modified graphene, Nat. Mater. 11 (2012) 203–207.
[97] H. Zhan, Y. Zhang, J.M. Bell, Y. Gu, Suppressed thermal conductivity of bilayer graphene with vacancy-initiated linkages, J. Phys. Chem. C 119 (2015) 1748–1752.
[98] Y.Y. Zhang, Y. Cheng, Q.X. Pei, C.M. Wang, Y. Xiang, Thermal conductivity of defective graphene, Phys. Lett. 376 (2012) 3668–3672.
[99] W. Huang, Q.-X. Pei, Z. Liu, Y.-W. Zhang, Thermal conductivity of fluorinated graphene: a non-equilibrium molecular dynamics study, Chem. Phys. Lett. 552 (2012) 97–101.
[100] Z.-X. Xie, K.-Q. Chen, W. Duan, Thermal transport by phonons in zigzag graphene nanoribbons with structural defects, J. Phys. Condens. Matter 23 (2011) 315302.
[101] J. Lan, Y. Cai, G. Zhang, J.-S. Wang, Y.-W. Zhang, Topological symmetry-induced width dependence of thermal conductance of edge-reconstructed graphene nanoribbons, J. Phys. D Appl. Phys. 47 (2014) 265303.
[102] Z. Guo, D. Zhang, X.-G. Gong, Thermal conductivity of graphene nanoribbons, Appl. Phys. Lett. 95 (2009) 163103.
[103] Y. Xu, X. Chen, B.-L. Gu, W. Duan, Intrinsic anisotropy of thermal conductance in graphene nanoribbons, Appl. Phys. Lett. 95 (2009) 233116.
[104] Y. Shen, G. Xie, X. Wei, K. Zhang, M. Tang, J. Zhong, G. Zhang, Y.-W. Zhang, Size and boundary scattering controlled contribution of spectral phonons to the thermal conductivity in graphene ribbons, J. Appl. Phys. 115 (2014) 063507.
[105] N. Wei, L. Xu, H.-Q. Wang, J.-C. Zheng, Strain engineering of thermal conductivity in graphene sheets and nanoribbons: a demonstration of magic flexibility, Nanotechnology 22 (2011) 105705.
[106] X. Li, K. Maute, M.L. Dunn, R. Yang, Strain effects on the thermal conductivity of nanostructures, Phys. Rev. B 81 (2010) 245318.
[107] X. Li, J. Chen, C. Yu, G. Zhang, Comparison of isotope effects on thermal conductivity of graphene nanoribbons and carbon nanotubes, Appl. Phys. Lett. 103 (2013) 013111.
[108] K. Watanabe, T. Taniguchi, H. Kanda, Direct-bandgap properties and evidence for ultraviolet lasing of hexagonal boron nitride single crystal, Nat. Mater. 3 (2004) 404–409.
[109] C.R. Dean, A.F. Young, I. Meric, C. Lee, L. Wang, S. Sorgenfrei, K. Watanabe, T. Taniguchi, P. Kim, K.L. Shepard, Boron nitride substrates for high-quality graphene electronics, Nat. Nanotechnol. 5 (2010) 722–726.
[110] C. Wang, J. Guo, L. Dong, A. Aiyiti, X. Xu, B. Li, Superior thermal conductivity in suspended bilayer hexagonal boron nitride, Sci. Rep. 6 (2016) 25334.
[111] E. Sichel, R. Miller, M. Abrahams, C. Buiocchi, Heat capacity and thermal conductivity of hexagonal pyrolytic boron nitride, Phys. Rev. B 13 (1976) 4607.
[112] L. Lindsay, D. Broido, Enhanced thermal conductivity and isotope effect in single-layer hexagonal boron nitride, Phys. Rev. B 84 (2011) 155421.
[113] L. Lindsay, D. Broido, Theory of thermal transport in multilayer hexagonal boron nitride and nanotubes, Phys. Rev. B 85 (2012) 035436.
[114] Q.H. Wang, K. Kalantar-Zadeh, A. Kis, J.N. Coleman, M.S. Strano, Electronics and optoelectronics of two-dimensional transition metal dichalcogenides, Nat. Nanotechnol. 7 (2012) 699–712.
[115] O. Lopez-Sanchez, D. Lembke, M. Kayci, A. Radenovic, A. Kis, Ultrasensitive photodetectors based on monolayer MoS_2, Nat. Nanotechnol. 8 (2013) 497–501.
[116] K.F. Mak, C. Lee, J. Hone, J. Shan, T.F. Heinz, Atomically thin MoS_2: a new direct-gap semiconductor, Phys. Rev. Lett. 105 (2010) 136805.
[117] A. Taube, J. Judek, A. Łapińska, M. Zdrojek, Temperature-dependent thermal properties of supported MoS_2 monolayers, ACS Appl. Mater. Interfaces 7 (2015) 5061–5065.
[118] R. Yan, J.R. Simpson, S. Bertolazzi, J. Brivio, M. Watson, X. Wu, A. Kis, T. Luo, A. R. Hight Walker, H.G. Xing, Thermal conductivity of monolayer molybdenum disulfide obtained from temperature-dependent raman spectroscopy, ACS Nano 8 (2014) 986–993.
[119] X. Gu, B. Li, R. Yang, Layer thickness-dependent phonon properties and thermal conductivity of MoS_2, J. Appl. Phys. 119 (2016) 085106.
[120] N. Peimyoo, J. Shang, W. Yang, Y. Wang, C. Cong, T. Yu, Thermal conductivity determination of suspended mono- and bilayer WS_2 by raman spectroscopy, Nano Res. 8 (2015) 1210–1221.
[121] N.T. Nguyen, P.A. Berseth, Q. Lin, C. Chiritescu, D.G. Cahill, A. Mavrokefalos, L. Shi, P. Zschack, M.D. Anderson, I.M. Anderson, Synthesis and properties of turbostratically disordered, ultrathin WSe_2 films, Chem. Mater. 22 (2010) 2750–2756.
[122] Z.-Y. Ong, G. Zhang, Y.W. Zhang, Anisotropic charged impurity-limited carrier mobility in monolayer phosphorene, J. Appl. Phys. 116 (2014) 214505.
[123] J. Dai, X.C. Zeng, Bilayer phosphorene: effect of stacking order on bandgap and its potential applications in thin-film solar cells, J. Phys. Chem. Lett. 5 (2014) 1289–1293.
[124] Y. Cai, G. Zhang, Y.-W. Zhang, Layer-dependent band alignment and work function of few-layer phosphorene, Sci. Rep. 4 (2014) 6677.
[125] W. Li, G. Zhang, Y.-W. Zhang, Electronic properties of edge-hydrogenated phosphorene nanoribbons: a first-principles study, J. Phys. Chem. C 118 (2014) 22368–22372.
[126] Z.-Y. Ong, Y. Cai, G. Zhang, Y.-W. Zhang, Strong thermal transport anisotropy and strain modulation in single-layer phosphorene, J. Phys. Chem. C 118 (2014) 25272–25277.
[127] W. Xu, L. Zhu, Y. Cai, G. Zhang, B. Li, Direction dependent thermal conductivity of monolayer phosphorene: parameterization of stillinger-weber potential and molecular dynamics study, J. Appl. Phys. 117 (2015) 214308.

[128] Y.-Y. Zhang, Q.-X. Pei, J.-W. Jiang, N. Wei, Y.-W. Zhang, Thermal conductivities of single- and multi-layer phosphorene: a molecular dynamics study, Nanoscale 8 (2016) 483–491.
[129] L. Zhu, G. Zhang, B. Li, Coexistence of size-dependent and size-independent thermal conductivities in phosphorene, Phys. Rev. B 90 (2014) 214302.
[130] A. Jain, A.J.H. McGaughey, Strongly anisotropic in-plane thermal transport in single-layer Black phosphorene, Sci. Rep. 5 (2015) 8501.
[131] Y. Zhang, W. Zhu, F. Hui, M. Lanza, T. Borca-Tasciuc, M. Muñoz Rojo, A review on principles and applications of scanning thermal microscopy (SThM), Adv. Funct. Mater. 30 (2020) 1900892.
[132] S. Xu, A. Fan, H. Wang, X. Zhang, X. Wang, Raman-based nanoscale thermal transport characterization: a critical review, Int. J. Heat Mass Transf. 154 (2020) 119751.
[133] X. Hou, F. Li, A. Fan, J. Xue, F. Zhang, Y. Zhang, W. Ma, X. Zhang, Mechanism and multiphysics simulation of edge hot-spot formation in GaN HEMTs: coupled thermo–electro–mechanical and trap-state effects, Int. J. Heat Mass Transf. 270 (2026) 129198.
[134] H. Wang, H. Zhu, G. Xue, H. Yang, Q. Guo, Z. Liu, K. Liu, B. Cao, Asymmetric thermal transport in a trilayer van der Waals heterostructure, Nat. Electron. 9 (2026) 747–757.
[135] Z.-Y. Liu, B.-Y. Cao, Discrete spectral Bayesian deconvolution for thermal parameter inversion in micro-nanoscale heterostructures, J. Appl. Phys. 137 (2025) 225102.
[136] Z.-K. Liu, Y. Shen, H.-L. Li, B.-Y. Cao, Observation of ballistic-diffusive thermal transport in GaN transistors using thermoreflectance thermal imaging, Rare Met. 43 (2024) 389–394.
[137] Y. Mao, H. Zhang, Y. Ma, H. Wang, H. Sun, C. Yuan, Multiwavelength laser-based transient thermoreflectance for channel-temperature monitoring of GaN HEMTs, IEEE Trans. Power Electron. 40 (2025) 8648–8657.
[138] G. Yang, B.-y. Cao, Three-sensor 3ω-2ω method for the simultaneous measurement of thermal conductivity and thermal boundary resistance in film-on-substrate heterostructures, J. Appl. Phys. 133 (2023) 045104.
[139] Y.-C. Hua, B.-Y. Cao, A two-sensor 3ω-2ω method for thermal boundary resistance measurement, J. Appl. Phys. 129 (2021) 125107.
[140] R. Mohan, S. Khan, R.B. Wilson, P.E. Hopkins, Time-domain thermoreflectance, Nat. Rev. Methods Primers 5 (2025) 55.
[141] P. Jiang, X. Qian, R. Yang, Tutorial: time-Domain thermoreflectance (TDTR) for thermal property characterization of bulk and thin film materials, J. Appl. Phys. 124 (2018) 161103.
[142] A.J. Schmidt, X. Chen, G. Chen, Pulse accumulation, radial heat conduction, and anisotropic thermal conductivity in pump-probe transient thermoreflectance, Rev. Sci. Instrum. 79 (2008) 114902.
[143] M. Fujii, X. Zhang, H. Xie, H. Ago, K. Takahashi, T. Ikuta, H. Abe, T. Shimizu, Measuring the thermal conductivity of a single carbon nanotube, Phys. Rev. Lett. 95 (2005) 065502.
[144] H. Wang, S. Hu, K. Takahashi, X. Zhang, H. Takamatsu, J. Chen, Experimental study of thermal rectification in suspended monolayer graphene, Nat. Commun. 8 (2017) 15843.
[145] J. Huang, A. Fan, X. Xia, S. Li, X. Zhang, In situ thermal conductivity measurement of single-crystal zeolitic imidazolate Framework-8 by raman-resistance temperature detectors method, ACS Nano 14 (2020) 14100–14107.
[146] F. Yao, S. Xia, H. Wei, J. Zheng, Z. Yuan, Y. Wang, B. Huang, D. Li, H. Lu, D. Xu, Experimental evidence of superdiffusive thermal transport in $Si_{0.4}Ge_{0.6}$ thin films, Nano Lett. 22 (2022) 6888–6894.
[147] Y. Zhang, Y. Du, X. Wan, M. An, A. Fan, F. Li, W. Ma, X. Zhang, Anomalous Enhancement of Thermal Conduction Across Twisted Van Der Waals Heterointerfaces, 123, Proceedings of the National Academy of Sciences, 2026 e2531049123.
[148] Z.-Y. Liu, Z.-K. Liu, G. Yang, B.-Y. Cao, Multi-pulse thermoreflectance imaging with structure function analyses for measuring thermophysical properties of microscale heterostructures, Int. J. Heat Mass Transf. 229 (2024) 125737.
[149] A. Cepellotti, G. Fugallo, L. Paulatto, M. Lazzeri, F. Mauri, N. Marzari, Phonon hydrodynamics in two-dimensional materials, Nat. Commun. 6 (2015) 6400.
[150] X. Huang, Y. Guo, Y. Wu, S. Masubuchi, K. Watanabe, T. Taniguchi, Z. Zhang, S. Volz, T. Machida, M. Nomura, Observation of phonon poiseuille flow in isotopically purified graphite ribbons, Nat. Commun. 14 (2023) 2044.
[151] X. Huang, R. Anufriev, L. Jalabert, K. Watanabe, T. Taniguchi, Y. Guo, Y. Ni, S. Volz, M. Nomura, A graphite thermal tesla valve driven by hydrodynamic phonon transport, Nature 634 (2024) 1086–1090.
[152] Z. Zhang, Y. Ouyang, Y. Cheng, J. Chen, N. Li, G. Zhang, Size-dependent phononic thermal transport in low-dimensional nanomaterials, Phys. Rep. 860 (2020) 1–26.
[153] R. Claes, S. Poncé, G.-M. Rignanese, G. Hautier, Phonon-limited electronic transport through first principles, Nat. Rev. Phys. 7 (2025) 73–90.
[154] S. Lu, Z. Zhang, S. Shan, Y. Li, P. Hänggi, J. Chen, Effect of spatial coherence on phonon transmission at interfaces, Phys. Rev. B 113 (2026) 165302.
[155] N. Li, J. Ren, L. Wang, G. Zhang, P. Hänggi, B. Li, Colloquium: phononics: manipulating heat flow with electronic analogs and beyond, Rev. Mod. Phys. 84 (2012) 1045–1066.
[156] B. Li, L. Wang, G. Casati, Thermal diode: rectification of heat flux, Phys. Rev. Lett. 93 (2004) 184301.
[157] Y. Wang, A. Vallabhaneni, J. Hu, B. Qiu, Y.P. Chen, X. Ruan, Phonon lateral confinement enables thermal rectification in asymmetric single-material nanostructures, Nano Lett. 14 (2014) 592–596.
[158] C. Zhang, M. An, Z. Guo, S. Chen, Perturbation theory of thermal rectification, Phys. Rev. 102 (2020) 042106.
[159] N. Yang, N. Li, L. Wang, B. Li, Thermal rectification and negative differential thermal resistance in lattices with mass gradient, Phys. Rev. B 76 (2007) 020301.
[160] Y. Zhang, Q. Lv, H. Wang, S. Zhao, Q. Xiong, R. Lv, X. Zhang, Simultaneous electrical and thermal rectification in a monolayer lateral heterojunction, Science 378 (2022) 169–175.
[161] S. Hu, M. An, N. Yang, B. Li, A series circuit of thermal rectifiers: an effective way to enhance rectification ratio, Small 13 (2017) 1602726.
[162] H. Liu, H. Wang, X. Zhang, A brief review on the recent experimental advances in thermal rectification at the nanoscale, Appl. Sci. (2019) 344.
[163] H. Ma, Z. Tian, Significantly high thermal rectification in an asymmetric polymer molecule driven by diffusive versus ballistic transport, Nano Lett. 18 (2018) 43–48.
[164] J. Zhu, K. Hippalgaonkar, S. Shen, K. Wang, Y. Abate, S. Lee, J. Wu, X. Yin, A. Majumdar, X. Zhang, Temperature-gated thermal rectifier for active heat flow control, Nano Lett. 14 (2014) 4867–4872.
[165] W. Ding, J. Guo, M. An, K. Tsuda, J. Shiomi, Human–AI collaboration for modeling heat conduction in nanostructures, npj Comput. Mater. 11 (2025) 158.
[166] W. Ren, P. Bøggild, J. Redwing, K.S. Novoselov, L. Sun, Y. Qi, K. Jia, Z. Liu, O. Burton, J. Alexander-Webber, S. Hofmann, Y. Cao, Y. Long, Q.-H. Yang, D. Li, S.H. Choi, K.K. Kim, Y.H. Lee, M. Li, Q. Huang, Y. Gogotsi, N. Clark, A. Carl, R. Gorbachev, T. Olsen, J. Rosen, K.S. Thygesen, D.K. Efetov, B.S. Jessen, M. Yankowitz, J. Barrier, R.K. Kumar, F.H.L. Koppens, H. Deng, X. Li, S. Dai, D. N. Basov, X. Wang, S. Das, X. Duan, Z. Yu, M. Borsch, A.C. Ferrari, R. Huber, M. Kira, F. Xia, X. Wang, Z.-S. Wu, X. Feng, P. Simon, H.-M. Cheng, B. Liu, Y. Xie, W. Jin, R.R. Nair, Y. Xu, Q. Zhang, A.K. Katiyar, J.-H. Ahn, I. Aharonovich, M. C. Hersam, S. Roche, Q. Hua, G. Shen, T. Ren, H.-B. Zhang, C.M. Koo, N. Koratkar, V. Pellegrini, R.J. Young, B. Qu, M. Lemme, A.J. Pollard, The 2D materials roadmap, 2D Mater. 13 (2026) 021501.
[167] L. Ponomarenko, A. Geim, A. Zhukov, R. Jalil, S. Morozov, K. Novoselov, I. Grigorieva, E. Hill, V. Cheianov, V. Fal'Ko, Tunable metal–insulator transition in double-layer graphene heterostructures, Nat. Phys. 7 (2011) 958–961.
[168] L. Britnell, R. Gorbachev, R. Jalil, B. Belle, F. Schedin, A. Mishchenko, T. Georgiou, M. Katsnelson, L. Eaves, S. Morozov, Field-effect tunneling transistor based on vertical graphene heterostructures, Science 335 (2012) 947–950.
[169] S.J. Haigh, A. Gholinia, R. Jalil, S. Romani, L. Britnell, D.C. Elias, K.S. Novoselov, L.A. Ponomarenko, A.K. Geim, R. Gorbachev, Cross-sectional imaging of individual layers and buried interfaces of graphene-based heterostructures and superlattices, Nat. Mater. 11 (2012) 764–767.
[170] S.-J. Liang, B. Cheng, X. Cui, F. Miao, Van der Waals heterostructures for high-performance device applications: challenges and opportunities, Adv. Mater. 32 (2020) 1903800.
[171] R. Moriya, T. Yamaguchi, Y. Inoue, Y. Sata, S. Morikawa, S. Masubuchi, T. Machida, (Invited) Vertical field effect transistor based on graphene/transition metal dichalcogenide van der Waals heterostructure, ECS Trans. 69 (2015) 357.
[172] Y. Wang, T. Li, Y. Li, R. Yang, G. Zhang, 2D-materials-based wearable biosensor systems, Biosensors (2022) 936.
[173] Y. Chen, Y. Wang, Z. Wang, Y. Gu, Y. Ye, X. Chai, J. Ye, Y. Chen, R. Xie, Y. Zhou, Z. Hu, Q. Li, L. Zhang, F. Wang, P. Wang, J. Miao, J. Wang, X. Chen, W. Lu, P. Zhou, W. Hu, Unipolar barrier photodetectors based on van der Waals heterostructures, Nat. Electron. 4 (2021) 357–363.
[174] J. Binder, J. Howarth, F. Withers, M.R. Molas, T. Taniguchi, K. Watanabe, C. Faugeras, A. Wysmolek, M. Danovich, V.I. Fal'ko, A.K. Geim, K.S. Novoselov, M. Potemski, A. Kozikov, Upconverted electroluminescence via Auger scattering of interlayer excitons in van der Waals heterostructures, Nat. Commun. 10 (2019) 2335.
[175] Z. Wang, D. Sapkota, T. Taniguchi, K. Watanabe, D. Mandrus, A.F. Morpurgo, Tunneling spin valves based on Fe_3GeTe_2/hBN/Fe_3GeTe_2 van der Waals heterostructures, Nano Lett. 18 (2018) 4303–4308.
[176] S. Jiang, L. Li, Z. Wang, J. Shan, K. Mak, Spin tunnel field-effect transistors based on two-dimensional van der Waals heterostructures, Nat. Electron. 2 (2019) 1.
[177] A. Sood, C. Sievers, Y.C. Shin, V. Chen, S. Chen, K.K.H. Smithe, S. Chatterjee, D. Donadio, K.E. Goodson, E. Pop, Engineering thermal transport across layered graphene–MoS_2 superlattices, ACS Nano 15 (2021) 19503–19512.
[178] J. Song, T. Miao, M. An, D. Chen, Modulation of thermal conductivity in graphene semi-encapsulated monolayer 2D β-bismuthene through twist angle engineering, Int. J. Heat Fluid Flow 117 (2026) 110033.
[179] N. Yang, J. Yue, X. Sun, Y. Liu, M. An, S. Hu, Anomalous thermal conductivity enhancement in twisted graphene/*h*-BN bilayers revealed by neuroevolution potential driven atomistic simulations, Phys. Rev. B 113 (2026) 035426.
[180] S. Tufail, H. Riggs, M. Tariq, A.I. Sarwat, Advancements and challenges in machine learning: a comprehensive review of models, libraries, applications, and algorithms, Electronics (2023) 1789.
[181] D. Willhelm, N. Wilson, R. Arroyave, X. Qian, T. Cagin, R. Pachter, X. Qian, Predicting van der Waals heterostructures by a combined machine learning and density functional theory approach, ACS Appl. Mater. Interfaces 14 (2022) 25907–25919.
[182] G.R. Schleder, C.M. Acosta, A. Fazzio, Exploring two-dimensional materials thermodynamic stability via machine learning, ACS Appl. Mater. Interfaces 12 (2020) 20149–20157.
[183] L. Zhu, J. Tang, B. Li, T. Hou, Y. Zhu, J. Zhou, Z. Wang, X. Zhu, Z. Yao, X. Cui, K. Watanabe, T. Taniguchi, Y. Li, Z.V. Han, W. Zhou, Y. Huang, Z. Liu, J.C. Hone, Y. Hao, Artificial neuron networks enabled identification and characterizations of 2D materials and van der Waals heterostructures, ACS Nano 16 (2022) 2721–2729.